Atmos. Chem. Phys. Discuss., doi:10.5194/acp-2016-314, 2016
Manuscript under review for journal Atmos. Chem. Phys.
Published: 11 May 2016

Atmospheric Chemistry and Physics Discussions

Emission-dominated gas exchange of elemental mercury vapor over natural surfaces in China

Xun Wang[1,2], Che-Jen Lin[1,3,4,*], Wei Yuan[1,2], Jonas Sommar [1], Wei Zhu [1], Xinbin Feng[1,*]

[1] State Key Laboratory of Environmental Geochemistry, Institute of Geochemistry, Chinese Academy of Sciences, Guiyang, China
[2] University of Chinese Academy of Sciences, Beijing, China
[3] Center for Advances in Water and Air Quality, Lamar University, Beaumont, TX, USA
[4] Department of Civil and Environmental Engineering, Lamar University, Beaumont, TX, USA

*** Corresponding Authors:**

Xinbin Feng
Phone: +86-851-5895728
Fax + 86-851-5891609
Email: fengxinbin@vip.skleg.cn

Che-Jen Lin
Phone: +1 409 880-8761
Fax: +1 409 880-8121
E-mail: Jerry.Lin@lamar.edu

Abstract: Mercury (Hg) emission from natural surfaces plays an important role in global Hg cycling. The present estimate of global natural emission has large uncertainty and remains unverified against field data, particularly for terrestrial surfaces. In this study, a mechanistic model is developed for estimating the emission of elemental mercury vapor (Hg^0) from natural surfaces in China. The development implements recent advancements in the understanding of air-soil and air-foliage exchange of Hg^0 and redox chemistry in soil and on surfaces, incorporates the effects of soil characteristics and landuse changes by agricultural activities, and is examined through a systematic set of sensitivity simulations. Using meteorology simulated by the Weather Research and Forecasting Model (WRF version 3.7), the exchange of Hg^0 between the atmosphere and natural surfaces in Mainland China is estimated to be 465.1 Mg yr^{-1}, including 565.5 Mg yr^{-1} of emission from soils, 9.0 Mg yr^{-1} of emission from water body, and 100.4 Mg yr^{-1} uptake by vegetation. The air-surface exchange is strongly dependent on the landuse and meteorology, with 9% of net emission from forest ecosystems, 50% from shrubland, and savanna and grassland, 33% from cropland, and 8% from other landuses. Given the large agricultural land area in China, farming activities play an important role on the air-surface exchange in farmland. Particularly, rice field shift from a net sink (3.3 Mg uptake) during April to October (rice planting) to a net source when the farmland is not flooded (November-March). Summing up emissions from each landuse, more than half of the total emission occurs in summer (51%), followed by spring (28%), autumn (13%) and winter (8%). Model verification is accomplished using observational data of air-soil/air-water fluxes and Hg deposition through litterfall for forest ecosystems in China and Monte Carlo simulations. In contrast to the earlier estimate by Shetty et al. (2008) that reported large emission from vegetative surfaces using an evapotranspiration approach, the estimate in this study shows natural emissions are primarily from grassland and dry cropland. Such an emission pattern may alter the current understanding of Hg emission outflow from China as reported by Lin et al. (2010b) because of a substantial natural Hg emission occurs in West China.

Atmos. Chem. Phys. Discuss., doi:10.5194/acp-2016-314, 2016
Manuscript under review for journal Atmos. Chem. Phys.
Published: 11 May 2016

Atmospheric Chemistry and Physics Discussions

1. Introduction

Accurate inventories of mercury (Hg) emission is the foundation for assessing Hg global biogeochemical cycling (Selin, 2009;Streets et al., 2009;Streets et al., 2011). Hg emission from anthropogenic sources has been quantified and updated with reasonable consistency since the 1990s (Streets et al., 2009;Streets et al., 2011;Zhang et al., 2015;Zhang et al., 2016). In particular, the inclusion of the release from commercial products and modifications of Hg emission speciation profiles dependent on implementation and upgrade of air pollution control technologies have substantially reduced the uncertainty level of anthropogenic Hg emission estimates(Horowitz et al., 2014;Zhang et al., 2016). In contrast, estimates of natural Hg emission are poorly constrained within large uncertainties (±2000 Mg yr^{-1}), limiting a comprehensive understanding of global/regional Hg cycling budgets (Pirrone et al., 2010;Wang et al., 2014b;Song et al., 2015). In light of the anticipated decrease of Hg emission from anthropogenic sources driven by the legally binding Minamata Convention (De Simone et al., 2015), a better quantification of natural Hg emission is critical in evaluating the effectiveness of policy actions (Selin, 2009;Pirrone et al., 2010;Song et al., 2015).

One of the challenges in predicting natural Hg emissions is to provide physical robust schemes for air-surface Hg^0 exchange. Such gas exchange schemes are complicated and involve not yet well understood processes in multiple environmental compartments, such as in terrestrial vegetative ecosystems. Thus, estimates from regression schemes obtained from correlations between Hg flux and environmental parameters (e.g., temperature, solar radiation, etc.) using limited datasets may not be representative (Xu et al., 1999;Bash et al., 2004;Lin et al., 2005;Gbor et al., 2006;Shetty et al., 2008;Selin et al., 2008;Smith-Downey et al., 2010) because relationship between measured fluxed and environmental parameters are based on limited field data that tend to be site-specific, which cannot account for the heterogeneity in soil properties and vegetative coverages. Although the bidirectional resistance schemes applied to describe the Hg^0 gas exchange may appropriate (Bash, 2010;Wang et al., 2014b;Wright and Zhang, 2015), they are limited by the availability of comprehensive soil property data and other physicochemical parameters such as Hg^{II} reduction kinetics and physical characteristics of interfacial exchanges(Bash, 2010;Wang et al., 2014b), leading to inconsistences between simulated and measured fluxes. Other challenges including

Atmos. Chem. Phys. Discuss., doi:10.5194/acp-2016-314, 2016
Manuscript under review for journal Atmos. Chem. Phys.
Published: 11 May 2016

68 acquiring and assimilating meteorology, landuse, and soil Hg and moisture content data into the model
69 scheme over a large geospatial coverage in China warrant for further model development to estimating
70 natural Hg emission (Wang et al., 2014b).

71 Advances in the fundamental understanding of Hg^{II} reduction provide new opportunities to build a
72 more physically robust air-soil exchange scheme. These include constrained pseudo-first-order reduction
73 rate constant of Hg^{II} in soil (10^{-11} to 10^{-10} s^{-1}, (Scholtz et al., 2003;Qureshi et al., 2011) and in natural water
74 (0.2-1.0 h^{-1}, O'Driscoll et al., 2006;Qureshi et al., 2010), where the UV-band of actinic light is a primary
75 driver for Hg^{II} photo-reduction in soils and water bodies rather than its visible part (Moore and Carpi,
76 2005;Si and Ariya, 2011). Besides constrained effective rate constants, the role of specific substructures
77 (e.g. functional groups such as -C(O)OH, -SH, -OH,) of DOM in the reduction mechanism has been
78 pinpointed by kinetic studies of various model compounds(He et al., 2012;Si and Ariya, 2011, 2015). In
79 some of these specific reactions, the presence of molecular oxygen shows an inhibiting role in the reduction
80 to Hg^0 whereas e.g. the photo-reduction of HgII bound to R-SH compounds proceeds to Hg^0 irrespective of
81 dissolved O_2 (Si and Ariya, 2011). For the photo-reduction in dry soil, the first-order rate constants are
82 0.007-0.028 h^{-1} for $HgCl_2$ coated over sand and 0.003-0.006 h^{-1} for Hg^{II} in a natural soil (Quinones and
83 Carpi, 2011). In the dark condition at room temperature (293 K), reduction rate constants of the reducible
84 Hg in soil are 0.001-0.002 h^{-1} (Pannu, 2012).

85 The intercontinental transport of Hg from China has been considered to significantly contribute to Hg
86 deposition in North America (Jaffe et al., 2005;Strode et al., 2008;Lin et al., 2010b;Chen et al., 2014). Wang
87 et al. (2014a) suggested the Hg emissions from natural and anthropogenic sources were comparable. Using
88 an outdated model scheme, Shetty et al. (2008) estimated 462 Mg yr^{-1} of Hg emitting into atmosphere in
89 China. This natural emission inventory has been used in East Asia CMAQ simulations to assess regional
90 Hg budgets (Lin et al., 2010b;Zhu et al., 2015a). However, the large uncertainty on the estimate of natural
91 Hg emission warrants a re-assessment of these earlier modeling efforts. In addition, the dataset of soil Hg
92 concentration in Shetty et al. (2008) is more than 3 decades old and requires updates to appropriately
93 represent spatially-resolved soil Hg contents that have been modified due to the rapid industrial
94 development and urbanization occurring in China since 1980s. In the meantime, the National Multi-Purpose

Atmos. Chem. Phys. Discuss., doi:10.5194/acp-2016-314, 2016
Manuscript under review for journal Atmos. Chem. Phys.
Published: 11 May 2016

Regional Geochemical Survey (NMPRGS) of China has been completed in 2014 (Li et al., 2014). This database provides soil Hg content for the agricultural and industrialized regions at resolution of 4 km, which forms a basis of greatly reducing the uncertainty of Hg natural emission previously hampered by data deficiency. In addition, a recent datasets of terrestrial flux in Mainland China reported in the literature allows verification of model results and optimization of model schemes. In particular, recent field measurements of Hg^0 air-surface exchange in China documented the flux characteristics over different land-uses including urban-rural-remote differences and effects of crop rotation over agricultural lands(Fu et al., 2008;Fu et al., 2010;Zhu et al., 2011;Fu et al., 2012;Fu et al., 2013a;Sommar et al., 2013a;Sommar et al., 2013b;Zhu et al., 2013;Sommar et al., 2015a;Zhu et al., 2016).

In light of the scientific advancements and renewed data availability discussed above, this work develops a state-of-the-science mechanistic model for estimating the natural Hg emission in China. For the first time, the simulated natural emission flux is verified with field measurements over different land surfaces in this modeling effort. The spatial, temporal and seasonal characteristics of the model-estimated emissions over soil, vegetative surface and water are presented and compared to the estimates performed by Shetty et al. (2008). The implications of the new natural emission estimate are discussed in terms of chemical transport of Hg emission in China and the need for a re-assessment of mercury emission outflow in China.

2. Methods

2.1 Model description

2.1.1 Reduction of Hg^{II} in soil

Based on Hg^{II} reduction mechanisms proposed in peer-reviewed literature(Moore and Carpi, 2005;Quinones and Carpi, 2011;Si and Ariya, 2011;Pannu, 2012), a new model scheme describing Hg^0 formation from Hg^{II} reduction in soil is developed using three reaction pathways: (1) photo-reduction of Hg^{II} in soil pore water (Hg_1^0), (2) photo-reduction Hg^{II} associated with soil particles (Hg_2^0), and (3) Hg^{II} reduction through non-photochemical pathways (Hg_3^0). The production of Hg^0 in surface soil is calculated as:

Atmos. Chem. Phys. Discuss., doi:10.5194/acp-2016-314, 2016
Manuscript under review for journal Atmos. Chem. Phys.
Published: 11 May 2016

Atmospheric Chemistry and Physics Discussions

$$\frac{dHg_1^0}{dt} = K_1 \cdot Hg_{s,m} \quad (1)$$

$$\frac{dHg_2^0}{dt} = K_2 \cdot Hg_{p,m} \quad (2)$$

$$\frac{dHg_3^0}{dt} = K_3 \cdot Hg_{t,m} \quad (3)$$

where K_1 is the photo-reduction rate constant of Hg^{II} in soil pore water (a comprehensive parameter list with units is shown in Table 1), K_2 is the photo-reduction rate constant of Hg^{II} associated with soil particles, K_3 is the Hg^{II} reduction rate constant in soil through non-photochemical pathways, $Hg_{s,m}$ is the Hg^{II} pool in soil pore water, $Hg_{p,m}$ is the labile Hg^{II} pool available for reduction in soil particles, $Hg_{t,m}$ is the total reducible Hg^{II} pool in soil. Based on the Arrhenius equation, K_1 and K_2 are parameterized as a function of solar irradiance and soil temperature, and K_3 is parameterized as the function of soil temperature and soil moisture:

$$K_1 = k_1 \cdot R \cdot \gamma \cdot e^{\frac{T-T_f}{T_f}\cdot\frac{E_a}{T}} \quad (4)$$

$$K_2 = k_2 \cdot R_i \cdot \gamma \cdot e^{\frac{T-T_f}{T_f}\cdot\frac{E_a}{T}} \quad (5)$$

$$K_3 = k_3 \cdot e^{\frac{T-T_f}{T_f}\cdot\frac{E_a}{T}} \cdot e^{\frac{\theta-\theta_f}{\theta_f}\cdot\frac{E_b}{\theta}} \quad (6)$$

where k_1 and k_2 are the photo-reduction rate constants at the reference soil temperature (T_f, Table 1). k_3 is the dark-reduction rate constant at the reference soil temperature and soil moisture (θ_f, Table 1). R and R_i are total solar radiation in the soil profile and under the canopy, respectively. γ is the ratio of UV over total solar radiation. An empirical rule suggests that a 10°C temperature rise doubles reaction rates for many chemical reactions near room temperature (Kissinger, 1957;Hood et al., 1975), which has been evinced to apply for Hg^{II} reduction in boreal soil (Pannu et al., 2014). In addition, Hg emission flux from soil substrate doubles in the dark for a 25% increase of soil moisture content (Lin et al., 2010a). Based on these observations, Equations 4-6 can be simplified as:

$$K_1 = k_1 \cdot R \cdot \gamma \cdot 2^{\frac{T-T_f}{10}} \quad (7)$$

$$K_2 = k_2 \cdot R_i \cdot \gamma \cdot 2^{\frac{T-T_f}{10}} \quad (8)$$

$$K_3 = k_3 \cdot 2^{\frac{T-T_f}{10}} \cdot 2^{\frac{\theta-\theta_f}{25\%}} \quad (9)$$

R and R_i in Equations 7-8 are calculated based on the Beer-Lambert law:

Atmos. Chem. Phys. Discuss., doi:10.5194/acp-2016-314, 2016
Manuscript under review for journal Atmos. Chem. Phys.
Published: 11 May 2016

Atmospheric Chemistry and Physics Discussions

$$R_i = R_0 \cdot e^{-K \cdot LAI} \quad (10)$$

$$R = R_i \cdot \int_0^l e^{-k_r \cdot l} dl \quad (11)$$

where R_0 is solar irradiance above the canopy, K is the canopy light extinction coefficient, LAI is leaf area index, k_r is the light extinction coefficient in soil, l is the depth of surface soil.

$Hg_{s,m}$ and $Hg_{p,m}$ and $Hg_{t,m}$ are calculated based on Lyon et al. (1997):

$$Hg_{s,m} = \frac{[Hg_t] \cdot BD}{\theta + kd \cdot BD} \cdot V \cdot \theta \cdot 10^6 \quad (12)$$

$$Hg_{p,m} = \frac{[Hg_t] \cdot BD \cdot kd}{\theta + kd \cdot BD} \cdot BD \cdot V \cdot \varphi \quad (13)$$

$$Hg_{t,m} = [Hg_t] \cdot BD \cdot V \cdot \varphi \quad (14)$$

where $[Hg_t]$ is the total Hg^{II} concentration in soil, BD is the soil bulk density, θ is the soil moisture, and V is the soil volume, φ is the ratio of reducible Hg over total Hg in soil. kd is the soil-water partition coefficient and calculated following Lee et al. (2001) and Sauve et al. (2000):

$$\log kd = r \cdot pH + s \cdot \log(1000 \cdot foc) + t \quad (15)$$

where f_{oc} is the fraction of organic carbon in surface soil. The values r, s and t are regression coefficients.

Following Obrist et al. (2014), we assume that the Hg^0 emission from soil is controlled by diffusion process after Hg^{II} reduction. Basing on the Fick's first law, the observed air-soil flux exchange can be calculated as:

$$F_{soil} = Hg_1^0 + Hg_2^0 + Hg_3^0 - D_{soil} \frac{GEM}{d/2} \Delta t \quad (16)$$

$$D_{soil} = 0.66 \cdot (\sigma - \theta) \cdot D_0 \quad (17)$$

where D_{soil} and D_0 are the Hg^0 vapor diffusion coefficient in soil and ambient air. GEM is the atmospheric Hg^0 concentration, σ is the soil porosity. Hence, during a time period Δt, the soil Hg^0 vapor compensation point used in bidirectional resistance model can be derived as:

$$\chi_g = \frac{(Hg_1^0 + Hg_2^0 + Hg_3^0) \cdot d/2}{D_{soil} \cdot \Delta t} \quad (18)$$

2.1.2 Updates for air-terrestrial exchanges

Extending from the two categories (vegetated surface canopy and bare land) considered in Wang et al. (2014b), the terrestrial system is divided into four categories: vegetated surface with unsaturated soil

Atmos. Chem. Phys. Discuss., doi:10.5194/acp-2016-314, 2016
Manuscript under review for journal Atmos. Chem. Phys.
Published: 11 May 2016

Atmospheric Chemistry and Physics Discussions

moisture (e.g., forest, grassland, shrubland, etc.), vegetated surface with saturated soil (i.e., rice paddy), barren or sparsely vegetated land, and snow/ice surface. The governing equation for calculating Hg^0 air-surface exchange over vegetated surfaces is:

$$F_{cnp} = \frac{\Delta t}{(R_a+R_b)}(\chi_{cnp} - C_{atm}) \quad (19)$$

where R_a is the aerodynamic resistance, R_b is the quasi-laminar sub-layer resistance, C_{atm} is the atmospheric Hg concentration, χ_{cnp} is the overall compensation point. For the canopy biomes with unsaturated soil, χ_{cnp} is parameterized as Wang et al. (2014b):

$$\chi_{cnp} = \frac{\frac{\chi_c}{R_c}+\frac{\chi_s}{R_s}+\frac{\chi_g}{R_g+R_{ac}}+\frac{C_{atm}}{R_a+R_b}}{\frac{1}{R_c}+\frac{1}{R_s}+\frac{1}{R_g+R_{ac}}+\frac{1}{R_a+R_b}} \quad (20)$$

where χ_c is the cuticular compensation point, χ_s is the stomatal compensation point, R_c is the cuticular resistance, R_s is the stomatal resistance, R_g is the soil diffusion resistance, R_{ac} is the in-canopy aerodynamic resistance (Table 1 in details). While for vegetated surface with saturate soil, χ_{cnp} is parameterized as following:

$$\chi_{cnp} = \frac{\frac{\chi_c}{R_c}+\frac{\chi_s}{R_s}+\frac{\chi_w}{R_w+R_{ac}}+\frac{C_{atm}}{R_a+R_b}}{\frac{1}{R_c}+\frac{1}{R_s}+\frac{1}{R_w+R_{ac}}+\frac{1}{R_a+R_b}} \quad (21)$$

where χ_w is the soil compensation point, R_w is the water diffusion resistance.

The governing equation for air-surface exchange in barren or sparsely vegetated land, and snow/ice surface is:

$$F_{bls} = \frac{\Delta t}{R_a+R_b+R_g}(\chi_g - C_{atm}) \quad (22)$$

For bare land, R_g is calculated following Zhang and Lindberg (1999):

$$R_g = \frac{d/2}{0.66\cdot(\sigma-\theta)\cdot D_0} \quad (23)$$

For snow/ice surface, R_g is evaluated following Zhang et al. (2012b):

$$\frac{1}{R_g} = \frac{\alpha_{Hg^0}}{R_{g(SO_2)}} + \frac{\beta_{Hg^0}}{R_{g(O_3)}} \quad (24)$$

where $R_{g(SO_2)}$ and $R_{g(O_3)}$ are the diffusion resistances of SO_2 and O_3, α_{Hg^0} is the Hg^0 scaling factor based on SO_2, β_{Hg^0} is Hg^0 scaling factor based on O_3. The formulation of $R_{g(SO_2)}$ and $R_{g(O_3)}$ has been described previously (Zhang et al., 2003;Wang et al., 2014b). χ_g is assumed to be 3 ng m^{-3} based on field

Atmos. Chem. Phys. Discuss., doi:10.5194/acp-2016-314, 2016
Manuscript under review for journal Atmos. Chem. Phys.
Published: 11 May 2016

196 measurements at air-snow interface (Mann et al., 2015;Lalonde et al., 2003;Fain et al., 2007;Maxwell et al.,
197 2013). Other parameters in Equations 19-24 are described in details in Wang et al. (2014b).

198 **2.2 Model configuration and data**

199 The modeling domain is in Lambert Conformal projection, with 223×149 grid cells at 36-km spatial
200 resolution. The modeling period is one year (2013). Hourly meteorological data are prepared using the
201 Weather Research and Forecasting (WRF) model Version 3.7. Sensitivity analysis in Wang et al. (2014b)
202 showed that accurate model representation of environmental parameters (e.g., temperature, solar irradiance,
203 etc.) greatly improves the flux estimate. To obtain the best physics and dynamics options of WRF for the
204 China domain, a $L_{25}(5^6)$ orthogonal design of experiments is utilized (Supplementary material, Table **S1**).
205 The best combination of meteorological physics options is selected based on model evaluation metrics R
206 (correlation coefficient) and RMSE (root-mean-square error) between simulated outputs of each
207 combination of options and observed values in 750 meteorological stations. The selected physics options
208 are Thompson (Microphysics Options), Betts-Miller-Janjic (Cumulus Parameterization Options), RRTMG
209 (Radiation Physics Options) and BouLac (PBL Physics Options) based on the results of meteorological
210 model performance evaluation (Figure **S1**).

211 The datasets for surface soil properties (1 km spatial resolution) containing organic matters contents,
212 pH, bulk density and porosity are adopted from Shangguan et al. (2013). The land cover data (1 km spatial
213 resolution) is obtained from Ran et al. (2012). The land cover map represents the best available datasets
214 and follows the IGBP (International Geosphere-Biosphere Programme) classification system (Figure **S2**).
215 The ratio of rice planting fields in China during each month are classified following the method used in Liu
216 et al. (2013). The rice planting seasons are April to October in South China (including double rice planting),
217 and May to October in Northeast China (single rice planting). The LAI data, also with a 1 km spatial
218 resolution, are adopted from Yuan et al. (2011). The soil Hg content information utilized by Shetty et al.
219 (2008) is updated and greatly expanded with the comprehensive NMPRGS dataset (Li et al., 2014). These
220 high resolution datasets were re-gridded into the domain specification for each landuse using the spatial
221 tools in ArcGIS 10.1. The soil Hg content varies with landuse types, containing 119±9~211±83, 61±33 ~

Atmos. Chem. Phys. Discuss., doi:10.5194/acp-2016-314, 2016
Manuscript under review for journal Atmos. Chem. Phys.
Published: 11 May 2016

197±96, 80±59~82±74, 80±59~82±74 and 31±15~162±83 of Hg for forest ecosystems, shrubland, savanna/grassland, cropland, and other landuses, respectively (Table 1).

In the simulation, the Hg^0 concentration retrieved from the output of the Hg extension of Community Multi-scale Air Quality modeling system (CMAQ-Hg) version 4.7 for the same modeling period is applied to represent the ambient air concentration of Hg^0 (Lin et al., 2010b). The simulation does not incorporate the feedback of the air-surface exchange to the air concentration because the feedback of the air-surface exchange to the air concentration does not significantly modify the atmospheric Hg^0 concentration, and the typical variation range of ambient Hg^0 concentration is not a sensitivity parameter for flux change (Wang et al., 2014b). The model algorithms are coded in FORTRAN 90 and Network Common Data Form (NetCDF) version 4.3. The gridded model results are visualized by the Visualization Environmental for Rich Data Interpretation (VERDI) version 1.5.

3 Results and discussion

3.1 Verification for soil Hg reduction scheme

Values of all model parameters used in the simulation are showed in Table 1. The value of k_1 is assumed to be 6×10^{-9} m^2 W^{-1} s^{-1} based on the relationship between radiant intensity and apparent photo-reduction rate constant in aerated solution observed by Si and Ariya (2011). Considering the 2 mm maximum photolysis penetration depth in soil (Hebert and Miller, 1990), the measured rate constant in soil particles (depth = 2.07 mm) from Quinones and Carpi (2011) is 2×10^{-3} m^2 W^{-1} h^{-1} (k_2) with respect to the pool of labile Hg^{II} available for reduction. The value of k_3 is assumed to be 1.0×10^{-3} h^{-1} based on the average rate constants for dark (thermal) reduction (Pannu, 2012). The mean ratio of reducible Hg in soil is assumed to be 0.03 for the soil with vegetation based on measurements from Pannu (2012). No data is available for the bare soil. Data from Lindberg et al. (1999) hints that Hg enriched desert soil (1400-5000 ng g^{-1} total Hg) produces a nominal Hg^0 efflux in the range from 40 to 60 ng m^{-2} h^{-1}. Derived from back-calculation taking pore diffusion into account, the fraction of reducible Hg is predicted at least 10 times lower (≤ 0.003) than that in the soil with vegetation.

Atmos. Chem. Phys. Discuss., doi:10.5194/acp-2016-314, 2016
Manuscript under review for journal Atmos. Chem. Phys.
Published: 11 May 2016

Atmospheric Chemistry and Physics Discussions

Sensitivity analyses using a box model for a typical forest soil are performed to gauge the selected rate coefficients and the results are showed in Figure 2. With $k_1 = 6.0\times10^{-9}$ m^2 W^{-1} s^{-1}, $k_2 = 2\times10^{-3}$ m^2 W^{-1} h^{-1}, $k_3 = 1.0\times10^{-3}$ h^{-1}, the Hg^0 vapor concentration in soil porous media is estimated to be 4.5 ng m^{-3}, comparable to the measured concentration (4.1±2.0 ng m^{-3}) in the surface forest floor (Moore and Castro, 2012), suggesting that the selected values for the empirical constants appropriately represent environmental condition. Generally, the range of Hg^0 vapor in all simulations is 1.5-6.7 ng m^{-3}. Less than 0.1% Hg^0 vapor is from photo-reduction in soil solution as the Hg pool in soil solution is small (⩽0.1% of total Hg concentration). A ~16% fraction of the pore Hg^0 concentration derives from thermal Hg^{II} reduction, contributing to 0.5-1 ng m^{-3} of Hg^0 vapor present in soil gas. Hg^0 soil gas concentrations are typically lower than atmospheric Hg concentration (1-2 ng m^{-3}) in forest ecosystems (Carpi and Lindberg, 1998;Ericksen and Gustin, 2006;Kuiken et al., 2008a;Kuiken et al., 2008b;Obrist et al., 2014;Fu et al., 2015) and suggest forest floor acting as a sink at night. This is consistent with the sign of nocturnal fluxes observed over forest floor settings (Carpi and Lindberg, 1998;Ericksen et al., 2006;Kuiken et al., 2008a;Kuiken et al., 2008b). Moore and Carpi (2005) reported that the Hg flux under sun-lit condition is 3-5 times higher than the value under dark condition. This developed model is capable of simulating such observation that the photo-reduction in soil particles dominates the formation of Hg^0 vapor.

Figure 3 illustrates the model response to the model variables at the two experimental levels in Table 2. Noting that the two experimental levels represent the typical endpoints of environmental parameter ranges and therefore the range of flux response to the possible variation of environmental factors can be measured. On average, increasing soil bulk density from 0.1 to 1.5 g cm^{-3}, and Hg content from 50 to 1000 ng g^{-1}, and soil temperature from 0 to 30 °C, and solar radiation from 0 to 1000 W m^{-2}, will significantly enhance the flux by 112-135 ng m^{-2} h^{-1}. Additional 112-128 ng m^{-2} h^{-1} synergistic effects from the combination of above parameters are also predicted. On the other hand, increasing leaf area index (LAI) from 0 to 7 m^2 m^{-2} reduces the flux by 131 ng m^{-2} h^{-1}. In addition, LAI could offset the positive effects from bulk density, soil Hg concentration, and solar radiation above canopy, leading to an additional -114 to -131 ng m^{-2} h^{-1} decrease, indicating that the canopy shading substantially constrains soil Hg evasion, consistent

Atmos. Chem. Phys. Discuss., doi:10.5194/acp-2016-314, 2016
Manuscript under review for journal Atmos. Chem. Phys.
Published: 11 May 2016

274 with the shading could decrease 70-90% fluxes compared to non-shaded soils in filed measurements (Carpi
275 and Lindberg, 1998;Zhang et al., 2001;Choi and Holsen, 2009).

276 Compared to the earlier sensitivity analysis in Wang et al. (2014b), the soil organic matter content
277 appear not to considerably influence the simulated flux (p = 0.915). In the new scheme, the soil organic
278 matter is not incorporated into either K_2 or K_3, in accordance with the findings of Pannu (2012). While Hg^0
279 evasion from substrates coated with $HgCl_2$ and humic matter is inversely correlated with humic matter
280 content both in the dark and under irradiation, the inhibitory effect from humic matter is not linear to its
281 content (Mauclair et al. (2008). For instance, relatively small differences are observed at humic matter
282 content > 1% (Mauclair et al., 2008). Additionally, the effect of soil organic matter type has not been
283 comprehensively investigated (Zhang and Lindberg, 1999;Bash et al., 2007). Further study to quantify the
284 corresponding reduction rate constants associated with different types of soil organic matters (or species)
285 and solar radiation, as well as field flux data that relate the observed flux intensity to a given type of organic
286 matter, can further improve the present model parameterization.
287
288 **3.2 Diurnal variation of natural Hg^0 emissions in China**
289 Table 3 shows the annual mean air-surface fluxes for different landuse types. Annual mean air-foliage
290 fluxes range from -0.2 to -4.5 ng m^{-2} h^{-1}, with the highest value over the woody savannas, and the lowest
291 over deciduous forests (Table 3). The diurnal variation for air-foliage flux is displayed in Figure 4. Higher
292 deposition occurs during early morning (8:00-10:00) and later afternoon (16:00-17:00) due to the suitable
293 air temperature and solar irradiance that induces Hg uptake by stomata. The rates of Hg uptake during
294 midday are comparatively weaker due to the stronger irradiance and higher temperature. This bimodal
295 pattern is consistent with field observations (Lindberg et al., 2002;Poissant et al., 2008;Fritsche et al.,
296 2008;Sommar et al., 2015a), suggesting that the model is capable of simulating the diurnal pattern of air-
297 foliage exchange of Hg^0. Such pattern in the modelling is caused by re-emission of the deposited Hg on the
298 surface foliage through photo-reduction under the strong solar radiation during noontime, and also the offset
299 effect from emissions from underlying soils. Except for urban lands, the strength of diurnal deposition for

Atmos. Chem. Phys. Discuss., doi:10.5194/acp-2016-314, 2016
Manuscript under review for journal Atmos. Chem. Phys.
Published: 11 May 2016

the other landuse is controlled by LAI, solar radiation, and air temperature. The elevated atmospheric Hg concentration is the important parameter to induce Hg uptake by growing foliage in urban lands.

Simulated mean air-soil fluxes range from 0.1 to 23.3 ng m^{-2} h^{-1}, with the lowest flux over barren vegetated lands and the highest over urban lands (Table 3). This suggests that the simulated air-soil fluxes greatly vary over different landuses. There are distinct diurnal variations in terrestrial ecosystems (Figure 5). Such diurnal pattern is caused by the variation of solar radiation, close to zero at night and peaking at 13:00 to 15:00 (UTC+8). Similar diurnal patterns have been observed during filed measurements for forest, grassland, and cropland in China (Feng et al., 2005;Fu et al., 2008;Fu et al., 2012;Zhu et al., 2013). The degree of diurnal variability for each landuse in terrestrial ecosystems is highly related to the LAI. Higher LAI gives a more intensive canopy shading and largely inhibits Hg evasion from soil under canopy. This is also the main reason for relative weaker diurnal variation over forest soils compared to shrubland, grassland and cropland (Figure 5). The synergistic interactions between low vegetation cover and high soil concentration (Mean=162±83 ng g^{-1}) results in the strongest diurnal variation for urban land-types.

The simulated annual mean air-water flux is 3.4 ng m^{-2} h^{-1}. The diurnal variability for air-water flux is weaker since wind speed is a more influential driver than sun-light (Wang et al., 2014b), consistent with the diurnal variation observed in field studies that meteorology and photochemical process are the primary factors(Feng et al., 2002;Feng et al., 2003;Wang et al., 2006;Feng et al., 2008;Fu et al., 2010;Fu et al., 2013a;Fu et al., 2013b).

Overall, the annual net natural emission in China is 465.1 Mg Hg (Table 3), including 565.5 Mg yr^{-1} of emission from soil, 9.0 Mg yr^{-1} of emission from water body, and 100.4 Mg yr^{-1} deposition (uptake) on vegetated landscapes. The annual quantity of emission from soil is comparable to the estimate (528 Mg yr^{-1}) based on the scale-up calculation using measured air-soil fluxes (Fu et al., 2015a) that suggest emissions from cropland and grassland are the most important contributor. Of the total Hg^0 emission estimated by the model, 50% is from shrubland, savanna and grassland (C6-C11, 38% total landuse); 33% is from cropland (C12-C13, 22% total landuse); 9% is from forest (C1-C5, 14% total landuse); and 8% is from other landuse types. The forest contributes to 28% of Hg uptake by foliage; shrubland, savanna and grassland contribute to 38%; cropland contributes to 33%; and other landuse types contribute to 1%.

Atmos. Chem. Phys. Discuss., doi:10.5194/acp-2016-314, 2016
Manuscript under review for journal Atmos. Chem. Phys.
Published: 11 May 2016

Atmospheric Chemistry and Physics Discussions

Although soil Hg contents in forest ecosystems are 2-4 times higher than that in grassland and cropland, total annual fluxes above the canopy (soil+foliage) of forest ecosystems are 1-6 times lower than the values in other two types of landuses (Table 3). This highlights the importance of canopy cover in natural emission process of Hg^0. It is noteworthy that the landuse data are based on the survey in 2000 (Ran et al., 2012). During last 15 years, the forested area in China increased from 14.0% to 21.6% (FAO, 2014), benefiting from implementation of governmental Grain for Green Project and stricter natural forest protection actions. Assuming that annual mean air-surface fluxes are at the same level as in this study, the total quantity of natural Hg emission in 2014 is approximately 5% smaller than this estimate because of the increasing forest coverage. Given the forest coverage is projected to be 24% in 2030, and 26% in 2050 (FAO, 2014), the total quantity of natural Hg emission in China during 2030-2050 would decrease 9-10 %.

3.3 Spatial distribution of natural Hg emission in China

The annual spatial distribution of air-foliage flux can be divided by the well-known geo-demographic demarcation line, "Heihe-Tengchong Line" (Figure 6.1). The vegetation on the east side of the line is much denser than on the west side of the line because of abundant annual precipitation (≥ 800 mm, Figure **S2**), which leads to much stronger Hg^0 uptake by vegetation (>90% of the grid cells have a flux below -1.0 ng m^{-2} h^{-1} on the east side, compared to >90% of the grid cells has a flux above -0.5 ng m^{-2} h^{-1} on the west side). There is an enhanced Hg deposition in South China (22˚N-27˚N,105˚E-113˚E, Figure 6.1) where fluxes ranging -3.8 to -19.1 ng m^{-2} h^{-1}. This can be explained by an elevation in atmospheric Hg concentrations and a more intense vegetative Hg^0 uptake. Field measurements suggest that this region has dense vegetation (i.e., high LAI, Figure **S3**) and elevated (2-10 ng m^{-3}) atmospheric Hg concentration (Fu et al., 2015;Zhu, 2014), which enhances Hg uptake by foliage. Specifically, evergreen broadleaf forest has the highest LAI compared to other type of forests (Liu et al., 2012) and shows enhanced Hg uptake (up to -4.5 ng m^{-2} h^{-1} mean flux). Although the direct measurement of Hg deposition flux through vegetative uptake is still not feasible presently, the measured Hg input through litterfall (Fu et al., 2015) suggested the rate of Hg uptake by foliage could up to 4-12 ng m^{-2} h^{-1}, comparable to the simulation results in this study.

Atmos. Chem. Phys. Discuss., doi:10.5194/acp-2016-314, 2016
Manuscript under review for journal Atmos. Chem. Phys.
Published: 11 May 2016

353 Figure 6.2 shows the spatial distribution of annual air-soil fluxes. There are three high flux regions
354 (mean flux ⩾ 10 ng m^{-2} h^{-1}): cropland/grassland in South and Southwest China (mainly in Guangdong,
355 Guangxi, Guizhou, Yunnan, Chongqing and Sichuan provinces), cropland in North China (Heibei, Henan,
356 and Shangdong provinces), and grassland in North China (Inner Mongolia, Shanxi, and Shaanxi, and
357 Xinjiang provinces). Such elevated fluxes in first two regions have been confirmed in field
358 observations(Feng et al., 2005;Wang et al., 2005;Wang et al., 2006;Fu et al., 2008;Sommar et al., 2015b).
359 Elevated fluxes in South and Southwest China are attributed to the elevated Hg concentration in soil (85%
360 of grid cells has a soil Hg content ⩾100 ng g-1, Figure 1). Interestingly, soil Hg content is not the primary
361 factor causing the high fluxes in the other two regions (70% of grid cells has a soil Hg content ⩽50 ng g-
362 1). Dry deposition of PBM and/or GOM plausibly supply to the reducible Hg in soil for gradual reduction
363 and volatilization as Hg^0 (Sommar et al., 2015b). The relatively low LAI (Figure S3), strong solar irradiance
364 and high soil temperature (Figure **S4-S5**) during summer/autumn contribute to the high simulated emissions.
365 The lower simulated fluxes in desert regions compared to fluxes over grassland (Figure 6.2) are caused by
366 the lower fraction of reducible Hg in soils.

367 Since the soil Hg^0 efflux is the primary source of natural Hg emission, the spatial distribution of the
368 natural Hg emission is strongly influenced by air-soil flux (Figure 7.1). There is a distinct seasonal variation
369 in the emission quantity: 8% in winter, 28% in spring, 51% in summer, and 13% in autumn (Figure 7.2-
370 7.5). Elevated fluxes mainly cluster in South and Southwest China in winter because of higher soil Hg
371 content (Figure 1), and relatively higher temperature and stronger irradiance. Highest correlation
372 coefficients are found between the flux and soil Hg concentration and soil bulk density (Table 4), suggesting
373 that the soil Hg^0 pool is a major factor influencing Hg emission in winter. From the cold to warm season,
374 fluxes gradually increase from low latitude to high latitude with the seasonal change of temperature and
375 solar radiation (Figure 7.2-7.4). Under the strong irradiance and temperatures during summer, >65% of the
376 grid cells in the domain has a flux above 10 ng m^{-2} h^{-1} and the effect of soil Hg content becomes weaker
377 (Table 4). In autumn, high flux occurs over the cropland of Central and North China, and over the regions
378 with high soil Hg content (Figure 7.6) because of the decreasing temperature and solar irradiance. Overall,

Atmos. Chem. Phys. Discuss., doi:10.5194/acp-2016-314, 2016
Manuscript under review for journal Atmos. Chem. Phys.
Published: 11 May 2016

379 72% of natural Hg emission occurs from May to September, with higher emission over grassland and
380 cropland in North China in these months.

381 It is worth noting that parts of regions in South China (23˚N-31˚N, 110˚E-120˚E, mainly in Fujian,
382 Jiangxi, Hunan, Hubei, and Anhui provinces) and Northeast China (39˚N-51˚N, 130˚E-134˚E, mainly in
383 Liaoning, Jilin and Heilongjiang provinces) have relatively lower fluxes (-6.9~9.0 ng m^{-2} h^{-1}) during
384 summer and autumn time (Figure 7.4-7.5). In addition to the impact from the intensive canopy cover in
385 forests (Figure **S2**), the agricultural activities in these regions also contribute to the smaller fluxes. Based
386 on Liu et al. (2013), 60% croplands in these regions are flooded for rice planting in summer and autumn.
387 Field-scale flux measurement using micrometeorological methods (i.e., aerodynamic gradient method)
388 suggest that a typical oilseeds-rice rotated cropland in Southwest China is a significant source during
389 oilseeds planting seasons with fluxes of 10.1-89.4 ng m^{-2} h^{-1}; and a mild sink during rice planting seasons
390 with fluxes of -3.4 to -15.8 ng m^{-2} h^{-1} (Zhu, 2014). The model also successfully simulates such a pattern,
391 with simulated fluxes at 1.1-101.5 ng m^{-2} h^{-1} (Figure 7.2-7.3) during winter and earlier spring when
392 croplands are not flooded and -3.5 to 1.5 ng m^{-2} h^{-1} during the rice growing season (Figure S6). Overall, 3.3
393 Mg Hg^0 is predicted to deposit into rice paddies during the rice growing season, with 56% of the deposition
394 occurring in summer, 41% in autumn, and 3% in late spring.
395
396 **3.4 Verification of model estimates**

397 For the first time, the simulated natural Hg emission in China is verified against field observational
398 data in this study. The dataset of Hg deposition through litterfall is utilized for verifying the simulated air-
399 foliage fluxes because of two reasons: (1) it has been shown that Hg deposition through litterfall dominates
400 dry deposition ($\geqslant$70%) in forests of China (Fu et al., 2015); and the annual Hg deposition through litterfall
401 has been used as a surrogate to constrain air-foliage fluxes in forest ecosystems (Risch et al., 2012;Zhang
402 et al., 2012a), and (2) the litterfall data in China have are more comprehensive for different forest types
403 compared to the air-foliage flux measured by enclosure methods. For verifying the exchange fluxes over
404 water and soil surfaces, the flux measurements over forest soil, grassland, cropland and water body in China
405 (Table **S2**) are utilized.

Atmos. Chem. Phys. Discuss., doi:10.5194/acp-2016-314, 2016
Manuscript under review for journal Atmos. Chem. Phys.
Published: 11 May 2016

Atmospheric Chemistry and Physics Discussions

406 To estimate the annual Hg deposition through litterfall in the study domain, Monte Carlo simulation
407 (described in details in SI) is applied for constructing the probability distribution of the litterfall deposition
408 based on litter biomass production and litterfall Hg concentration in China reported in peer-reviewed
409 literature (Figure 8). The sampling locations include 20 sites in Tibetan Plateau, 27 sites for evergreen
410 forests, and 12 sites for deciduous forests. The quality-assured data of litter biomass production (number of
411 replicates $\geqslant$ 3, collector size = 1 m^2) are obtained from the China National Knowledge Infrastructure
412 (CNKI). This dataset includes the measurements at 5 sites in Tibetan Plateau, 277 sites for evergreen forests,
413 74 sites for deciduous forests, and 61 sites for mixed forests.

414 Figure 8 shows the dataset of Hg concentration in litterfall. The Hg concentration for evergreen forest
415 ranges from 17 to 120 ng g^{-1} with a mean of 52±26 ng g^{-1}. For deciduous forest, the range is 21-62 ng g^{-1}
416 with a mean of 38±12 ng g^{-1}. The difference between the concentration observed in evergreen forests and
417 in deciduous forests is significant (paired *t* test, $p < 0.05$). The Hg concentration in litters for deciduous
418 forest in China is compared to the values reported for the same forest type in Europe and North America (p
419 = 0.101). Hg deposition through litterfall in evergreen broadleaf forest (C2) range from 26 to 72 μg m^{-2} y^{-1}
420 (n=5 sites) with a mean of 43±27 μg m^{-2} y^{-1} (Fu et al., 2015;Ma et al., 2015;Wang et al., 2009), consistent
421 with the Hg deposition estimated by Monte Carlo simulation (mean=37±19 μg m^{-2} y^{-1}; 95% confidence
422 interval is 4-89 μg m^{-2} y^{-1}). The model-estimated Hg deposition for C1, C3, C4, and C5 is 22±10, 15±7,
423 16±11, and 17±8 μg m^{-2} y^{-1}, respectively.

424 The measured air-soil flux (Table **S2**) ranges from -1.4 to 20.7 ng m^{-2} h^{-1} over forest soil (n=19; mean=
425 6.1±5.1 ng m^{-2} h^{-1}), from -18.7 to 114 ng m^{-2} h^{-1} over grassland (n=14; mean= 26±36 ng m^{-2} h^{-1}), from -4.1
426 to 135 ng m^{-2} h^{-1} over cropland (n=33; mean= 21.3±36.7 ng m^{-2} h^{-1}). For water body (n=51), the flux range
427 is 0-43.8 ng m^{-2} h^{-1} with a mean of 4.6±6.6 ng m^{-2} h^{-1} (Table **S2**). The mean flux in the warm season (May
428 to October) is substantially higher than those in the cold seasons: 3.3 times for water surface (p=0.004), 3.2
429 times higher for forest soil (p=0.08), and 1.4 times for cropland (p=0.50). A reverse trend is found for
430 grassland, which has higher mean flux in cold seasons (50% higher, p=0.36).

431 Figure 9.1 compares the model estimate and the mean and uncertainty level estimated by Monte Carlo
432 simulation using field data. The annual Hg uptake simulated by the bidirectional exchange model is not

Atmos. Chem. Phys. Discuss., doi:10.5194/acp-2016-314, 2016
Manuscript under review for journal Atmos. Chem. Phys.
Published: 11 May 2016

433 significantly different from the field observations ($p>0.05$, t-test), demonstrating the model capability for
434 simulating the air-foliage flux. Figure 9.2 shows the scatter plot of the measured versus model predicted
435 flux over soil and water ($R^2=0.73$). Modeling results for soil/water surfaces and over soil under forest
436 canopy also agree with filed measurements (Figure 9.3-9.4). The simulation somewhat underestimates the
437 high fluxes ($\geqslant$ 30 ng m^{-2} h^{-1}, Figure 9.2) measured over grassland and cropland (Figure 9.4).
438 The underestimated fluxes over grassland and cropland can be attributed to several possible reasons.
439 One is the bias caused by the comparatively coarser spatial resolution (36 km) of meteorological parameters
440 and soil properties that limit the reproduction of the instantaneously measured fluxes at observational sites.
441 In addition, the kinetic constants observed by laboratory study are used in the simulation for grassland and
442 cropland and potentially introduce uncertainty. Further studies focusing on in-situ measurement of Hg^{II}
443 reduction rate in soil can help constrain the model simulation result. Furthermore, limited mechanistic
444 understanding on Hg dry deposition (Gustin et al., 2015) and on the fate of deposited Hg (Lindberg et al.,
445 2007;Gustin et al., 2008b;Gustin et al., 2015;Ariya et al., 2015) complicates quantifying the contribution
446 of dry deposition to Hg emission from soil. Finally, the uncertainties caused by flux quantification
447 methodology (Lin et al., 2012;Zhu et al., 2015b, c) and the typically short transient campaign periods
448 (mostly ranging from several days to a couple of weeks) can also be a factor(Feng et al., 2005;Fu et al.,
449 2008;Fu et al., 2012;Fu et al., 2015;Zhu et al., 2015b, c). Improvement on flux methods and extended
450 campaign periods at more study sites for cropland/grassland will improve the model estimates.
451
452 **3.5 Comparison with earlier estimates and implications on Hg emission outflow in China**
453 Figures **S7** and **S8** show the gridded natural Hg emission in the East Asian Domain reported by Shetty
454 et al. (2008) and Wang et al. (2014a), which have two distinct differences compared to the new model
455 estimate in this study. One is regarding the role of vegetation in natural Hg emission, the other is spatial
456 distribution of the emission. Vegetation is clearly assigned as a substantial sink of Hg^0 based on the
457 mechanistic model algorithms in this study; and the shading of vegetation suppress Hg evasion from soil
458 under canopy. In contrast, vegetation is considered a major source, accounting for 76% total emissions in
459 Shetty et al. (2008) because earlier models treat Hg evasion similar to the evapotranspiration process that

Atmos. Chem. Phys. Discuss., doi:10.5194/acp-2016-314, 2016
Manuscript under review for journal Atmos. Chem. Phys.
Published: 11 May 2016

460 transport Hg from root zone through vascular tissues in foliage (Gbor et al., 2007;Shetty et al., 2008).
461 However, recent experimental evidence using stable Hg isotope tracers points to exclusion of this pathway
462 for cereal plants (Cui et al., 2014). In addition, Hg isotopic signatures in air and foliage samples (Demers
463 et al., 2013;Yin et al., 2013) and during air-foliage exchange process (Graydon et al., 2006;Gustin et al.,
464 2008a) indicate uptake of atmospheric Hg by foliage, pointing to vegetation as a Hg^0 sink. Also in contrast
465 to the spatial distribution of the emission in this study, earlier Hg^0 emission estimates occur mainly in the
466 regions on the east side of the "Heihe-Tengchong Line" (Shetty et al., 2008;Wang et al., 2014a). Such spatial
467 distribution in Shetty et al. (2008) is caused by spatial distribution of vegetation as the vegetation is the
468 most important contributor for Hg emission, and in Wang et al. (2014a) is caused by spatial distribution of
469 soil Hg concentration as soil Hg concentration shapes natural Hg emission in simple regression schemes.
470 Furthermore, this study advances upon the earlier estimates (Shetty et al., 2008;Wang et al., 2014a) in
471 two fronts. Firstly, the recent soil survey data including soil Hg content and other soil characteristics is a
472 major advantage in this study. The soil Hg data applied in Shetty et al. (2008) is outdated with a coarse
473 spatial resolution; while the data in Wang et al. (2014a) is based on the output of the global terrestrial Hg
474 model in GEOS-Chem, calculated from Hg/C ratios. In addition, the mechanistic model scheme that
475 comprehensively treats the meteorological parameters and physicochemical properties of soil represents the
476 air-surface exchange more appropriately compared to the earlier, undeveloped regression schemes (Shetty
477 et al., 2008;Wang et al., 2014a). With the model results verified against the field flux measurements, the
478 natural emission quantity and spatial distribution in this study represent the state of science estimate of air-
479 surface exchange of Hg^0 in China.
480 Although the total quantity of annual natural emission estimated by the new model developed in this
481 study is comparable to in earlier estimates (400-600 Mg yr^{-1}) by Shetty et al. (2008) and Wang et al. (2014a),
482 the distinct spatial distribution of natural emissions simulated in this study may alter the current
483 understanding of Hg emission outflow from China as reported by Lin et al. (2010b). The outflow of Hg
484 emissions in China is mainly driven by the prevailing west-wind drift (Lin et al., 2010b;Chen et al., 2014).
485 The larger natural Hg emission in the west side of model domain results in a longer residence time of evaded
486 Hg, which can be more readily oxidized and then deposited within the domain. Furthermore, the dense

Atmos. Chem. Phys. Discuss., doi:10.5194/acp-2016-314, 2016
Manuscript under review for journal Atmos. Chem. Phys.
Published: 11 May 2016

487 vegetation in the east side of the domain also enhance the uptake of atmospheric Hg^0. Such a spatial pattern
488 may lead to substantially larger domestic deposition and smaller quantity of outflow compared to the modes
489 estimates by Lin et al. (2010). We are presently to reassess the emission outflow using a regional chemical
490 transport model (e.g., CMAQ-Hg) and a similar mass balance approach by Lin et al. (2010); and will report
491 the model results in a future paper.
492
493 **4. Conclusions**
494 Using a mechanistic model incorporating the present state of understanding in Hg transformation in
495 soils and on foliage surface with up-to-date datasets of soil characteristics and landuse changes, the natural
496 emission of elemental mercury vapor in China is estimated to be 465.1 Mg yr^{-1}, including 565.5 Mg yr^{-1} of
497 emission from soils, 9.0 Mg yr^{-1} of emission from water bodies, and -100.4 Mg yr^{-1} deposition (uptake) by
498 vegetation. The air-surface exchange is strongly dependent on landuse and meteorology, with 9% of net
499 emission from forest ecosystems, 50% from shrubland, savanna and grassland, 33% from cropland, and 8%
500 from other landuses. Given the large agricultural land area in China, farming activities play an important
501 role on the air-surface exchange. Particularly, rice fields shift from a net sink (3.3 Mg uptake) during the
502 growing season in rice paddy to a net source during the season when the farmland is not flooded. The
503 estimated natural Hg^0 emission in this study yields similar Hg^0 evasion quantity but exhibits contrasting
504 spatial distribution compared to the estimate by Shetty et al. (2008). The difference in the spatial emission
505 patterns may alter the current understanding of Hg emission outflow from China as reported by Lin et al.
506 (2010b) because of a substantial amount of natural Hg^0 emission occurs in West China.
507 For future model improvement, studies focusing on fundamental understanding of Hg^{II} reduction in
508 soil (especially the role of soil organic matter, contribution of photochemical and non-chemical pathways,
509 and radiation transfer in soil) and air-vegetation exchange mechanisms are needed. Continuous
510 improvement on the data quality of soil characteristics and Hg content is also essential. Availability of field
511 data for modeling performance evaluation is also important for constraining the model. In particular, data
512 of air-foliage flux, and air-soil flux over cropland and grassland in the remote regions of North China is
513 also valuable for model calibration.
514

Atmospheric Chemistry and Physics Discussions

Acknowledgements

This work was funded by National "973" Program of China (2013CB430003), and State Key Laboratory of Environmental Geochemistry, IGCAS. The funding support is gratefully acknowledged.

References

Ariya, P. A., Amyot, M., Dastoor, A., Deeds, D., Feinberg, A., Kos, G., Poulain, A., Ryjkov, A., Semeniuk, K., Subir, M., and Toyota, K.: Mercury Physicochemical and Biogeochemical Transformation in the Atmosphere and at Atmospheric Interfaces: A Review and Future Directions, Chem Rev, 115, 3760-3802, 2015.

Bash, J. O., Miller, D. R., Meyer, T. H., and Bresnahan, P. A.: Northeast United States and Southeast Canada natural mercury emissions estimated with a surface emission model, Atmos Environ, 38, 5683-5692, 2004.

Bash, J. O., Bresnahan, P., and Miller, D. R.: Dynamic surface interface exchanges of mercury: A review and compartmentalized modeling framework, Journal of Applied Meteorology and Climatology, 46, 1606-1618, 10.1175/jam2553.1, 2007.

Bash, J. O.: Description and initial simulation of a dynamic bidirectional air-surface exchange model for mercury in Community Multiscale Air Quality (CMAQ) model, J Geophys Res-Atmos, 115, 2010.

Blackwell, B. D., Driscoll, C. T., Maxwell, J. A., and Holsen, T. M.: Changing climate alters inputs and pathways of mercury deposition to forested ecosystems, Biogeochemistry, 119, 215-228, 2014.

Carpi, A., and Lindberg, S. E.: Application of a Teflon (TM) dynamic flux chamber for quantifying soil mercury flux: Tests and results over background soil, Atmos Environ, 32, 873-882, 1998.

Chen, L., Wang, H. H., Liu, J. F., Tong, Y. D., Ou, L. B., Zhang, W., Hu, D., Chen, C., and Wang, X. J.: Intercontinental transport and deposition patterns of atmospheric mercury from anthropogenic emissions, Atmos Chem Phys, 14, 10163-10176, 2014.

Choi, H. D., and Holsen, T. M.: Gaseous mercury fluxes from the forest floor of the Adirondacks, Environmental Pollution, 157, 592-600, 2009.

Ciani, A., Goss, K. U., and Schwarzenbach, R. P.: Light penetration in soil and particulate minerals, Eur J Soil Sci, 56, 561-574, 2005.

Cui, L., Feng, X., Lin, C.-J., Wang, X., Meng, B., Wang, X., and Wang, H.: Accumulation and translocation of ^{198}Hg in four crop species, Environ Toxicol Chem, 33, 334-340, 2014.

De Simone, F., Cinnirella, S., Gencarelli, C. N., Yang, X., Hedgecock, I. M., and Pirrone, N.: Model Study of Global Mercury Deposition from Biomass Burning, Environ Sci Technol, 49, 6712-6721, 2015.

Demers, J. D., Blum, J. D., and Zak, D. R.: Mercury isotopes in a forested ecosystem: Implications for air-surface exchange dynamics and the global mercury cycle, Global Biogeochemical Cycles, 27, 222-238, 10.1002/gbc.20021, 2013.

Ericksen, J., and Gustin, M. S.: Air-surface exchange of mercury with soils amended with ash materials, J Air Waste Manage, 56, 977-992, 2006.

Ericksen, J. A., Gustin, M. S., Xin, M., Weisberg, P. J., and Fernandez, G. C. J.: Air-soil exchange of mercury from background soils in the United States, Sci Total Environ, 366, 851-863, 2006.

Fain, X., Grangeon, S., Bahlmann, E., Fritsche, J., Obrist, D., Dommergue, A., Ferrari, C. P., Cairns, W., Ebinghaus, R., Barbante, C., Cescon, P., and Boutron, C.: Diurnal production of gaseous mercury in the alpine snowpack before snowmelt, J Geophys Res-Atmos, 112, 2007.

FAO: State of the World's Forests 2014, FOOD AND AGRICULTURE ORGANIZATION OF THE UNITED NATIONS, Rome,

556 93-100, 2014.
557 Feng, X., Qiu, G., Wang, S., and Shang, L.: Distribution and speciation of mercury in surface waters in mercury mining
558 areas in Wanshan, Southwestern China, J Phys Iv, 107, 455-458, 2003.
559 Feng, X. B., Sommar, J., Gardfeldt, K., and Lindqvist, O.: Exchange flux of total gaseous mercury between air and
560 natural water surfaces in summer season, Sci China Ser D, 45, 211-220, 2002.
561 Feng, X. B., Wang, S. F., Qiu, G. A., Hou, Y. M., and Tang, S. L.: Total gaseous mercury emissions from soil in Guiyang,
562 Guizhou, China, J Geophys Res-Atmos, 110, 2005.
563 Feng, X. B., Wang, S. F., Qiu, G. G., He, T. R., Li, G. H., Li, Z. G., and Shang, L. H.: Total gaseous mercury exchange
564 between water and air during cloudy weather conditions over Hongfeng Reservoir, Guizhou, China, J Geophys Res-
565 Atmos, 113, 2008.
566 Fritsche, J., Wohlfahrt, G., Ammann, C., Zeeman, M., Hammerle, A., Obrist, D., and Alewell, C.: Summertime
567 elemental mercury exchange of temperate grasslands on an ecosystem-scale, Atmospheric Chemistry and Physics, 8,
568 2008.
569 Fu, X. W., Feng, X. B., and Wang, S. F.: Exchange fluxes of Hg between surfaces and atmosphere in the eastern flank
570 of Mount Gongga, Sichuan province, southwestern China, Journal of Geophysical Research-Atmospheres, 113, 2008.
571 Fu, X. W., Feng, X. B., Zhang, G., Xu, W. H., Li, X. D., Yao, H., Liang, P., Li, J., Sommar, J., Yin, R. S., and Liu, N.: Mercury
572 in the marine boundary layer and seawater of the South China Sea: Concentrations, sea/air flux, and implication for
573 land outflow, J Geophys Res-Atmos, 115, 2010.
574 Fu, X. W., Feng, X. B., Zhang, H., Yu, B., and Chen, L. G.: Mercury emissions from natural surfaces highly impacted by
575 human activities in Guangzhou province, South China, Atmos Environ, 54, 185-193, 2012.
576 Fu, X. W., Feng, X. B., Guo, Y. N., Meng, B., Yin, R. S., and Yao, H.: Distribution and production of reactive mercury and
577 dissolved gaseous mercury in surface waters and water/air mercury flux in reservoirs on Wujiang River, Southwest
578 China, J Geophys Res-Atmos, 118, 3905-3917, 2013a.
579 Fu, X. W., Feng, X. B., Yin, R. S., and Zhang, H.: Diurnal variations of total mercury, reactive mercury, and dissolved
580 gaseous mercury concentrations and water/air mercury flux in warm and cold seasons from freshwaters of
581 southwestern China, Environ Toxicol Chem, 32, 2256-2265, 2013b.
582 Fu, X. W., Zhang, H., Wang, X., Yu, B., Lin, C.-J., and Feng, X. B.: Observations of atmospheric mercury in China: a
583 critical review, Atmos. Chem. Phys. Discuss., 11925-11983, doi:10.5194/acpd-15-11925-2015, 2015.
584 Gbor, P. K., Wen, D. Y., Meng, F., Yang, F. Q., Zhang, B. N., and Sloan, J. J.: Improved model for mercury emission,
585 transport and deposition, Atmospheric Environment, 40, 973-983, DOI 10.1016/j.atmosenv.2005.10.040, 2006.
586 Gbor, P. K., Wen, D. Y., Meng, F., Yang, F. Q., and Sloan, J. J.: Modeling of mercury emission, transport and deposition
587 in North America, Atmospheric Environment, 41, 1135-1149, DOI 10.1016/j.atmosenv.2006.10.005, 2007.
588 Graydon, J. A., St Louis, V. L., Lindberg, S. E., Hintelmann, H., and Krabbenhoft, D. P.: Investigation of mercury exchange
589 between forest canopy vegetation and the atmosphere using a new dynamic chamber, Environ Sci Technol, 40, 4680-
590 4688, 2006.
591 Gustin, M. S., Lindberg, S. E., and Weisberg, P. J.: An update on the natural sources and sinks of atmospheric mercury,
592 Appl Geochem, 23, 482-493, 2008a.
593 Gustin, M. S., Lindberg, S. E., and Weisberg, P. J.: An update on the natural sources and sinks of atmospheric mercury,
594 Applied Geochemistry, 23, 10.1016/j.apgeochem.2007.12.010, 2008b.
595 Gustin, M. S., Amos, H. M., Huang, J., Miller, M. B., and Heidecorn, K.: Measuring and modeling mercury in the
596 atmosphere: a critical review, Atmos Chem Phys, 15, 5697-5713, 2015.

597 He, F., Zheng, W., Liang, L. Y., and Gu, B. H.: Mercury photolytic transformation affected by low-molecular-weight
598 natural organics in water, Sci Total Environ, 416, 429-435, 2012.
599 Hebert, V. R., and Miller, G. C.: Depth dependence of direct and indirect photolysis on soil surfaces, J. Agric. Food
600 Chem., 38, 913-918, DOI: 10.1021/jf00093a069, 1990.
601 Hood, A., Gutjahr, C. C. M., and Heacock, R. L.: Organic Metamorphism and the Generation of Petroleum, AAPG
602 BULLETIN, 59, 986-996, 1975.
603 Horowitz, H. M., Jacob, D. J., Amos, H. M., Streets, D. G., and Sunderland, E. M.: Historical Mercury Releases from
604 Commercial Products: Global Environmental Implications, Environmental Science & Technology, 48, 10242-10250,
605 2014.
606 Jaffe, D., Prestbo, E., Swartzendruber, P., Weiss-Penzias, P., Kato, S., Takami, A., Hatakeyama, S., and Kajii, Y.: Export
607 of atmospheric mercury from Asia, Atmos Environ, 39, 3029-3038, 2005.
608 Juillerat, J. I., Ross, D. S., and Bank, M. S.: Mercury in litterfall and upper soil horizons in forested ecosystems in
609 Vermont, USA, Environmental Toxicology and Chemistry, 31, 10.1002/etc.1896, 2012.
610 Kissinger, H. E.: Reaction Kinetics in Differential Thermal Analysis, The Journal of Physical Chemistry 29, 1702-1706,
611 DOI: 10.1021/ac60131a045, 1957.
612 Kuiken, T., Gustin, M., Zhang, H., Lindberg, S., and Sedinger, B.: Mercury emission from terrestrial background
613 surfaces in the eastern USA. II: Air/surface exchange of mercury within forests from South Carolina to New England,
614 Appl Geochem, 23, 356-368, 2008a.
615 Kuiken, T., Zhang, H., Gustin, M., and Lindberg, S.: Mercury emission from terrestrial background surfaces in the
616 eastern USA. Part I: Air/surface exchange of mercury within a southeastern deciduous forest (Tennessee) over one
617 year, Appl Geochem, 23, 345-355, 2008b.
618 Laacouri, A., Nater, E. A., and Kolka, R. K.: Distribution and Uptake Dynamics of Mercury in Leaves of Common
619 Deciduous Tree Species in Minnesota, USA, Environ Sci Technol, 47, 10462-10470, 2013.
620 Lalonde, J. D., Amyot, M., Doyon, M. R., and Auclair, J. C.: Photo-induced Hg(II) reduction in snow from the remote
621 and temperate Experimental Lakes Area (Ontario, Canada), Journal of Geophysical Research-Atmospheres, 108, Artn
622 4200
623 Doi 10.1029/2001jd001534, 2003.
624 Lee, S. Z., Chang, L., Chen, C. M., Tsai, Y. I., and Liu, M. C.: Predicting soil-water partition coefficients for Hg(II) from
625 soil properties, Water Sci Technol, 43, 187-196, 2001.
626 Li, M., Xi, X. H., Xiao, G. Y., Cheng, H. X., Yang, Z. F., Zhou, G. H., Ye, J. Y., and Li, Z. H.: National multi-purpose regional
627 geochemical survey in China, J Geochem Explor, 139, 21-30, 2014.
628 Lin, C.-J., Gustin, M. S., Singhasuk, P., Eckley, C., and Miller, M.: Empirical Models for Estimating Mercury Flux from
629 Soils, Environmental Science & Technology, 44, 8522-8528, 10.1021/es1021735, 2010a.
630 Lin, C. J., Lindberg, S. E., Ho, T. C., and Jang, C.: Development of a processor in BEIS3 for estimating vegetative mercury
631 emission in the continental United States, Atmos Environ, 39, 7529-7540, 2005.
632 Lin, C. J., Pan, L., Streets, D. G., Shetty, S. K., Jang, C., Feng, X., Chu, H. W., and Ho, T. C.: Estimating mercury emission
633 outflow from East Asia using CMAQ-Hg, Atmos Chem Phys, 10, 1853-1864, 2010b.
634 Lin, C. J., Zhu, W., Li, X. C., Feng, X. B., Sommar, J., and Shang, L. H.: Novel Dynamic Flux Chamber for Measuring Air-
635 Surface Exchange of Hg-o from Soils, Environmental Science & Technology, 46, 8910-8920, Doi 10.1021/Es3012386,
636 2012.
637 Lindberg, S. E., Zhang, H., Gustin, M., Vette, A., Marsik, F., Owens, J., Casimir, A., Ebinghaus, R., Edwards, G., Fitzgerald,

638 C., Kemp, J., Kock, H. H., London, J., Majewski, M., Poissant, L., Pilote, M., Rasmussen, P., Schaedlich, F., Schneeberger,
639 D., Sommar, J., Turner, R., Wallschlager, D., and Xiao, Z.: Increases in mercury emissions from desert soils in response
640 to rainfall and irrigation, J Geophys Res-Atmos, 104, 21879-21888, 1999.
641 Lindberg, S. E., Dong, W. J., and Meyers, T.: Transpiration of gaseous elemental mercury through vegetation in a
642 subtropical wetland in Florida, Atmos Environ, 36, 5207-5219, 2002.
643 Lindberg, S. E., Bullock, R., Ebinghaus, R., Engstrom, D., Feng, X. B., Fitzgerald, W., Pirrone, N., Prestbo, E., and
644 Seigneur, C.: A synthesis of progress and uncertainties in attributing the sources of mercury in deposition, Ambio, 36,
645 19-32, 2007.
646 Liu, L., Xu, X. L., Zhuang, D. F., Chen, X., and Li, S.: Changes in the Potential Multiple Cropping System in Response to
647 Climate Change in China from 1960-2010, Plos One, 8, 2013.
648 Liu, Y. B., Ju, W. M., Chen, J. M., Zhu, G. L., Xing, B. L., Zhu, J. F., and He, M. Z.: Spatial and temporal variations of forest
649 LAI in China during 2000-2010, Chinese Science Bulletin, 57, 2846-2856, 2012.
650 Lyon, B. F., Ambrose, R., Rice, G., and Maxwell, C. J.: Calculation of soil-water and benthic sediment partition
651 coefficients for mercury, Chemosphere, 35, 791-808, 1997.
652 Ma, M., Wang, D. Y., Du, h. X., Z, Z., and W, S. Q.: Atmospheric mercury deposition and its contribution of the regional
653 atmospheric transport to mercury pollution at a national forest nature reserve, southwest China, Environ Sci Pollut
654 R, DOI 10.1007/s11356-015-5152-9, 2015.
655 Mann, E. A., Mallory, M. L., Ziegler, S. E., Avery, T. S., Tordon, R., and O'Driscoll, N. J.: Photoreducible Mercury Loss
656 from Arctic Snow Is Influenced by Temperature and Snow Age, Environmental Science & Technology, 49, 12120-12126,
657 2015.
658 Mauclair, C., Layshock, J., and Carpi, A.: Quantifying the effect of humic matter on the emission of mercury from
659 artificial soil surfaces, Appl Geochem, 23, 594-601, 2008.
660 Maxwell, J. A., Holsen, T. M., and Mondal, S.: Gaseous Elemental Mercury (GEM) Emissions from Snow Surfaces in
661 Northern New York, Plos One, 8, 2013.
662 Moan, J.: 7 Visible Light and UV Radiation, Radiation, 69, 2001.
663 Moore, C., and Carpi, A.: Mechanisms of the emission of mercury from soil: Role of UV radiation, J Geophys Res-
664 Atmos, 110, 2005.
665 Moore, C. W., and Castro, M. S.: Investigation of factors affecting gaseous mercury concentrations in soils, Science of
666 the Total Environment, 419, 136-143, 2012.
667 Niu, Z., Zhang, X., Wang, Z., and Ci, Z.: Mercury in leaf litter in typical suburban and urban broadleaf forests in China,
668 J Environ Sci-China, 23, 2042-2048, 10.1016/s1001-0742(10)60669-9, 2011.
669 Obrist, D., Pokharel, A. K., and Moore, C.: Vertical Profile Measurements of Soil Air Suggest Immobilization of Gaseous
670 Elemental Mercury in Mineral Soil, Environ Sci Technol, 48, 2242-2252, 2014.
671 Pannu, R.: QUANTIFYING MERCURY REDUCTION KINETICS IN SOILS, Degree of Doctor of Philosophy, Department of
672 Soil Science, University of Saskatchewan, 156 pp., 2012.
673 Pannu, R., Siciliano, S. D., and O'Driscoll, N. J.: Quantifying the effects of soil temperature, moisture and sterilization
674 on elemental mercury formation in boreal soils, Environmental Pollution, 193, 138-146, 2014.
675 Pirrone, N., Cinnirella, S., Feng, X., Finkelman, R. B., Friedli, H. R., Leaner, J., Mason, R., Mukherjee, A. B., Stracher, G.
676 B., Streets, D. G., and Telmer, K.: Global mercury emissions to the atmosphere from anthropogenic and natural
677 sources, Atmos Chem Phys, 10, 5951-5964, 2010.
678 Poissant, L., Pilote, M., Yumvihoze, E., and Lean, D.: Mercury concentrations and foliage/atmosphere fluxes in a maple

679 forest ecosystem in Quebec, Canada, Journal of Geophysical Research-Atmospheres, 113, 10.1029/2007jd009510,
680 2008.
681 Quinones, J. L., and Carpi, A.: An Investigation of the Kinetic Processes Influencing Mercury Emissions from Sand and
682 Soil Samples of Varying Thickness, Journal of Environmental Quality, 40, 647-652, 10.2134/jeq2010.0327, 2011.
683 Qureshi, A., MacLeod, M., and Hungerbuhler, K.: Quantifying uncertainties in the global mass balance of mercury,
684 Global Biogeochemical Cycles, 25, GB4012, Gb4012, 10.1029/2011gb004068, 2011.
685 Ran, Y. H., Li, X., Lu, L., and Li, Z. Y.: Large-scale land cover mapping with the integration of multi-source information
686 based on the Dempster-Shafer theory, Int J Geogr Inf Sci, 26, 169-191, 2012.
687 Risch, M. R., DeWild, J. F., Krabbenhoft, D. P., Kolka, R. K., and Zhang, L. M.: Litterfall mercury dry deposition in the
688 eastern USA, Environ Pollut, 161, 284-290, 2012.
689 Sauve, S., Hendershot, W., and Allen, H. E.: Solid-solution partitioning of metals in contaminated soils: Dependence
690 on pH, total metal burden, and organic matter, Environmental Science & Technology, 34, 1125-1131, 2000.
691 Scholtz, M. T., Van Heyst, B. J., and Schroeder, W.: Modelling of mercury emissions from background soils, Science of
692 the Total Environment, 304, 185-207, 10.1016/s0048-9697(02)00568-5, 2003.
693 Selin, N. E., Jacob, D. J., Yantosca, R. M., Strode, S., Jaegle, L., and Sunderland, E. M.: Global 3-D land-ocean-
694 atmosphere model for mercury: Present-day versus preindustrial cycles and anthropogenic enrichment factors for
695 deposition (vol 22, artn no GB3099, 2008), Global Biogeochem Cy, 22, 2008.
696 Selin, N. E.: Global Biogeochemical Cycling of Mercury: A Review, Annu Rev Env Resour, 34, 43-63, 2009.
697 Selvendiran, P., Driscoll, C. T., Montesdeoca, M. R., and Bushey, J. T.: Inputs, storage, and transport of total and methyl
698 mercury in two temperate forest wetlands, J Geophys Res-Biogeo, 113, 2008.
699 Shangguan, W., Dai, Y., Liu, B., Zhu, A., Duan, Q., Wu, L., Ji, D., Ye, A., Yuan, H., Zhang, Q., Chen, D., Chen, M., Chu, J.,
700 Dou, Y., Guo, J., Li, H., Li, J., Liang, L., Liang, X., Liu, H., Liu, S., Miao, C., and Zhang, Y.: A China data set of soil properties
701 for land surface modeling, J Adv Model Earth Sy, 5, 212-224, 10.1002/jame.20026, 2013.
702 Shetty, S. K., Lin, C. J., Streets, D. G., and Jang, C.: Model estimate of mercury emission from natural sources in East
703 Asia, Atmos Environ, 42, 8674-8685, 2008.
704 Si, L., and Ariya, P. A.: Aqueous photoreduction of oxidized mercury species in presence of selected alkanethiols,
705 Chemosphere, 84, 1079-1084, 2011.
706 Si, L., and Ariya, P. A.: Photochemical reactions of divalent mercury with thioglycolic acid: Formation of mercuric
707 sulfide particles, Chemosphere, 119, 467-472, 2015.
708 Smith-Downey, N. V., Sunderland, E. M., and Jacob, D. J.: Anthropogenic impacts on global storage and emissions of
709 mercury from terrestrial soils: Insights from a new global model, Journal of Geophysical Research-Biogeosciences,
710 115, Artn G03008
711 Doi 10.1029/2009jg001124, 2010.
712 Sommar, J., Zhu, W., Lin, C. J., and Feng, X. B.: Field Approaches to Measure Hg Exchange Between Natural Surfaces
713 and the Atmosphere A Review, Critical Reviews in Environmental Science and Technology, 43, 1657-1739, Doi
714 10.1080/10643389.2012.671733, 2013a.
715 Sommar, J., Zhu, W., Shang, L. H., Feng, X. B., and Lin, C. J.: A whole-air relaxed eddy accumulation measurement
716 system for sampling vertical vapour exchange of elemental mercury, Tellus B, 65, 2013b.
717 Sommar, J., Zhu, W., Shang, L., Lin, C. J., and Feng, X. B.: Seasonal variations in metallic mercury (Hg0) vapor exchange
718 over biannual wheat – corn rotation cropland in the North China Plain, Biogeosciences Discuss., 12, 16105-
719 16158, 2015a.

720 Sommar, J., Zhu, W., Shang, L., Lin, C. J., and Feng, X. B.: Seasonal variations in metallic mercury (Hg0) vapor exchange
721 over biannual wheat - corn rotation cropland in the North China Plain, Biogeosciences Discussions, 12, 16105-16158,
722 2015b.
723 Song, S., Selin, N. E., Soerensen, A. L., Angot, H., Artz, R., Brooks, S., Brunke, E. G., Conley, G., Dommergue, A.,
724 Ebinghaus, R., Holsen, T. M., Jaffe, D. A., Kang, S., Kelley, P., Luke, W. T., Magand, O., Marumoto, K., Pfaffhuber, K. A.,
725 Ren, X., Sheu, G. R., Slemr, F., Warneke, T., Weigelt, A., Weiss-Penzias, P., Wip, D. C., and Zhang, Q.: Top-down
726 constraints on atmospheric mercury emissions and implications for global biogeochemical cycling, Atmos Chem Phys,
727 15, 7103-7125, 2015.
728 Streets, D. G., Zhang, Q., and Wu, Y.: Projections of Global Mercury Emissions in 2050, Environmental Science &
729 Technology, 43, 2983-2988, Doi 10.1021/Es802474j, 2009.
730 Streets, D. G., Devane, M. K., Lu, Z. F., Bond, T. C., Sunderland, E. M., and Jacob, D. J.: All-Time Releases of Mercury
731 to the Atmosphere from Human Activities, Environmental Science & Technology, 45, 10485-10491, Doi
732 10.1021/Es202765m, 2011.
733 Strode, S. A., Jaegle, L., Jaffe, D. A., Swartzendruber, P. C., Selin, N. E., Holmes, C., and Yantosca, R. M.: Trans-Pacific
734 transport of mercury, J Geophys Res-Atmos, 113, 2008.
735 Tang, R., Wang, H., Luo, J., Sun, S., Gong, Y., She, J., Chen, Y., Dandan, Y., and Zhou, J.: Spatial distribution and temporal
736 trends of mercury and arsenic in remote timberline coniferous forests, eastern of the Tibet Plateau, China, Environ
737 Sci Pollut R, 22, 11658-11668, 10.1007/s11356-015-4441-7, 2015.
738 Wang, D. Y., He, L., Shi, X. J., Wei, S. Q., and Feng, X. B.: Release flux of mercury from different environmental surfaces
739 in Chongqing, China, Chemosphere, 64, 1845-1854, 2006.
740 Wang, S., Zhang, L., Wang, L., Wu, Q., Wang, F., and Hao, J.: A review of atmospheric mercury emissions, pollution
741 and control in China, Frontiers of Environmental Science & Engineering, 8, 631-649, 10.1007/s11783-014-0673-x,
742 2014a.
743 Wang, S. F., Feng, X. B., Qiu, G. L., Wei, Z. Q., and Xiao, T. F.: Mercury emission to atmosphere from Lanmuchang Hg-
744 Tl mining area, Southwestern Guizhou, China, Atmos Environ, 39, 7459-7473, 2005.
745 Wang, X., Lin, C. J., and Feng, X.: Sensitivity analysis of an updated bidirectional air-surface exchange model for
746 elemental mercury vapor, Atmos Chem Phys, 14, 6273-6287, 2014b.
747 Wang, Z. W., Zhang, X. S., Xiao, J. S., Zhijia, C., and Yu, P. Z.: Mercury fluxes and pools in three subtropical forested
748 catchments, southwest China, Environ Pollut, 157, 801-808, 2009.
749 Wright, L. P., and Zhang, L. M.: An approach estimating bidirectional air-surface exchange for gaseous elemental
750 mercury at AMNet sites, J Adv Model Earth Sy, 7, 35-49, 2015.
751 Xu, X. H., Yang, X. S., Miller, D. R., Helble, J. J., and Carley, R. J.: Formulation of bi-directional atmosphere-surface
752 exchanges of elemental mercury, Atmospheric Environment, 33, 4345-4355, Doi 10.1016/S1352-2310(99)00245-9,
753 1999.
754 Yin, R., Feng, X., and Meng, B.: Stable Hg Isotope Variation in Rice Plants (Oryza sativa L.) from the Wanshan Hg
755 Mining District, SW China, Environ. Sci. Technol., 2013.
756 Yuan, H., Dai, Y. J., Xiao, Z. Q., Ji, D. Y., and Shangguan, W.: Reprocessing the MODIS Leaf Area Index products for land
757 surface and climate modelling, Remote Sens Environ, 115, 1171-1187, 2011.
758 Zhang, H., and Lindberg, S. E.: Processes influencing the emission of mercury from soils: A conceptual model, J
759 Geophys Res-Atmos, 104, 21889-21896, 1999.
760 Zhang, H., Lindberg, S. E., and Gustin, M. S.: Nature of diel trend of mercury emission from soil: Current understanding

761 and hypotheses., Abstr Pap Am Chem S, 222, U429-U429, 2001.
762 Zhang, L., Brook, J. R., and Vet, R.: A revised parameterization for gaseous dry deposition in air-quality models,
763 Atmospheric Chemistry and Physics, 3, 2067-2082, 2003.
764 Zhang, L., Blanchard, P., Gay, D. A., Prestbo, E. M., Risch, M. R., Johnson, D., Narayan, J., Zsolway, R., Holsen, T. M.,
765 Miller, E. K., Castro, M. S., Graydon, J. A., St Louis, V. L., and Dalziel, J.: Estimation of speciated and total mercury dry
766 deposition at monitoring locations in eastern and central North America, Atmos Chem Phys, 12, 4327-4340, 2012a.
767 Zhang, L., Blanchard, P., Johnson, D., Dastoor, A., Ryzhkov, A., Lin, C. J., Vijayaraghavan, K., Gay, D., Holsen, T. M.,
768 Huang, J., Graydon, J. A., St Louis, V. L., Castro, M. S., Miller, E. K., Marsik, F., Lu, J., Poissant, L., Pilote, M., and Zhang,
769 K. M.: Assessment of modeled mercury dry deposition over the Great Lakes region, Environ Pollut, 161, 272-283,
770 2012b.
771 Zhang, L., Wang, S. X., Wang, L., Wu, Y., Duan, L., Wu, Q. R., Wang, F. Y., Yang, M., Yang, H., Hao, J. M., and Liu, X.:
772 Updated Emission Inventories for Speciated Atmospheric Mercury from Anthropogenic Sources in China, Environ Sci
773 Technol, 49, 3185-3194, 2015.
774 Zhang, L. X., Hu, Z. M., Fan, J. W., Zhou, D. C., and Tang, F. P.: A meta-analysis of the canopy light extinction coefficient
775 in terrestrial ecosystems, Frontiers of Earth Science, 8, 599-609, 2014.
776 Zhang, Y., Jacob, D. J., Horowitz, H. M., Chen, L., Amos, H. M., Krabbenhoft, D. P., Slemr, F., St. Louis, V. L., and
777 Sunderland, E. M.: Observed decrease in atmospheric mercury explained by global decline in anthropogenic
778 emissions, Proceedings of the National Academy of Sciences, 10.1073/pnas.1516312113, 2016.
779 Zhou, J., Feng, X. B., Liu, H. Y., Zhang, H., Fu, X. W., Bao, Z. D., Wang, X., and Zhang, Y. P.: Examination of total mercury
780 inputs by precipitation and litterfall in a remote upland forest of Southwestern China, Atmos Environ, 81, 364-372,
781 2013.
782 Zhu, J., Wang, D., Liu, X., and Zhang, Y.: Mercury fluxes from air/surface interfaces in paddy field and dry land, Applied
783 Geochemistry, 26, 10.1016/j.apgeochem.2010.11.025, 2011.
784 Zhu, J., Wang, T., Bieser, J., and Matthias, V.: Source attribution and process analysis for atmospheric mercury in
785 eastern China simulated by CMAQ-Hg, Atmospheric Chemistry and Physics, 15, 8767-8779, 2015a.
786 Zhu, J. S., Wang, D. Y., and Ma, M.: Mercury release flux and its influencing factors at the air-water interface in paddy
787 field in Chongqing, China, Chinese Sci Bull, 58, 266-274, 2013.
788 Zhu, W.: Deployment and Evaluation of Enclosure and Micrometeorological Techniques for Quantifying Air-surface
789 Exchange of Gaseous Elemental Mercury over Agricultural Lands, Doctor of Natural Science, University of Chinese
790 Academy of Sciences, University of Chinese Academy of Sciences, 169 pp., 2014.
791 Zhu, W., Sommar, J., Lin, C. J., and Feng, X.: Mercury vapor air-surface exchange measured by collocated
792 micrometeorological and enclosure methods - Part I: Data comparability and method characteristics, Atmos Chem
793 Phys, 15, 685-702, 2015b.
794 Zhu, W., Sommar, J., Lin, C. J., and Feng, X.: Mercury vapor air-surface exchange measured by collocated
795 micrometeorological and enclosure methods - Part II: Bias and uncertainty analysis, Atmos Chem Phys, 15, 5359-
796 5376, 2015c.
797 Zhu, W., Lin, C. J., Wang, X., Sommar, J., Fu, X., and Feng, X.: Global observations and modeling of atmosphere–surface
798 exchange of elemental mercury: a critical review, Atmos. Chem. Phys., 16, 4451-4480, 10.5194/acp-16-4451-2016,
799 2016.
800
801

Atmos. Chem. Phys. Discuss., doi:10.5194/acp-2016-314, 2016
Manuscript under review for journal Atmos. Chem. Phys.
Published: 11 May 2016

Atmospheric Chemistry and Physics Discussions

802

803 Table 1 Model variables, constants and rate coefficients used in the model simulation.

804

Term	Description	Values/units	References/Sources
Hg_1^0	Hg^0 formed by photo-reduction in solution	ng m^{-2} h^{-1}	
Hg_2^0	Hg^0 formed by photo-reduction in particles	ng m^{-2} h^{-1}	
Hg_3^0	Hg^0 formed by the dark-reduction in soil	ng m^{-2} h^{-1}	
K_1	Photo-reduction rate in soil solution	s^{-1}	
K_2	Photo-reduction rate constant in particles	s^{-1}	
K_3	Dark-reduction rate constant in soil	s^{-1}	
$Hg_{s,m}$	Hg^{II} pool in soil pore water	ng m^{-2}	
$Hg_{p,m}$	Reducible Hg^{II} pool in soil particles	ng m^{-2}	
$Hg_{t,m}$	Total reducible Hg^{II} pool in soil	ng m^{-2}	
T	Temperature	K	WRF
θ	Soil moisture	%	WRF
R	Total solar radiation	W m^{-2}	WRF
BD	Soil bulk density	g cm^{-3}	(Shangguan et al., 2013)
LAI	Leaf area index	m^2 m^{-2}	WRF (Yuan et al., 2011)
$[Hg_t]$	Total Hg^{II} concentration in soil	ng g^{-1}	
V	Soil volume	m^3	
kd	soil-water partition coefficient	L kg^{-1}	
GEM	Atmospheric Hg^0 concentration	ng m^{-3}	(Lin et al., 2010b)
σ	Soil porosity	%	(Shangguan et al., 2013)
D_{soil}	Hg^0 vapor diffusion coefficient in soil	m^2 s^{-1}	
D_0	Hg^0 vapor diffusion coefficient in ambient air	1.31×10^{-5} m^2 s^{-1}	(Scholtz et al., 2003)
F_{cnp}	The flux over canopy biomes	ng m^{-2} h^{-1}	
Δt	Time duration	s	
R_a	Aerodynamic resistance	s m^{-1}	(Wang et al., 2014b;Zhang et al., 2012b)
R_b	Quasi-laminar sub-layer resistance	s m^{-1}	Wang et al., 2014b;Zhang et al., 2012b)
C_{atm}	Atmospheric Hg concentration	ng m^{-3}	Wang et al., 2014b;Zhang et al., 2012b)
χ_{cnp}	The total compensation point	ng m^{-3}	Wang et al., 2014b;Zhang et al., 2012b)
χ_c	Cuticular interfaces compensation point	ng m^{-3}	Wang et al., 2014b;Zhang et al., 2012b)
χ_s	Stomatal interfaces compensation point	ng m^{-3}	Wang et al., 2014b;Zhang et al., 2012b)
χ_g	Soil interfaces compensation point	ng m^{-3}	Wang et al., 2014b;Zhang et al., 2012b)
R_c	cuticular resistance	s m^{-1}	Wang et al., 2014b;Zhang et al., 2012b)
R_s	stomatal resistance	s m^{-1}	Wang et al., 2014b;Zhang et al., 2012b)
R_g	soil diffusion resistance	s m^{-1}	Wang et al., 2014b;Zhang et al., 2012b)
R_w	water diffusion resistance	s m^{-1}	Wang et al., 2014b;Zhang et al., 2012b)
$R_{g(SO_2)}$	SO_2 soil diffusion resistance	s m^{-1}	Wang et al., 2014b;Zhang et al., 2012b)
$R_{g(O_3)}$	O_3 soil diffusion resistance	s m^{-1}	Wang et al., 2014b;Zhang et al., 2012b)
d	Light penetration into soil column	2 mm	(Hebert and Miller, 1990)

Atmos. Chem. Phys. Discuss., doi:10.5194/acp-2016-314, 2016
Manuscript under review for journal Atmos. Chem. Phys.
Published: 11 May 2016

Atmospheric Chemistry and Physics Discussions

γ	Ratio of UV radiation over total radiation	0.08	(Moan, 2001)
K	Canopy light extinction coefficient	0.56	(Zhang et al., 2014)
k_r	Light extinction coefficient in soil	3 mm^{-1}	(Ciani et al., 2005)
k_1	Photo-reduction rate constant in soil solution	6×10^{-9} m^2 W^{-1} s^{-1}	(Si and Ariya, 2011)
k_2	Photo-reduction rate constant in soil particles	2×10^{-3} m^2 W^{-1} h^{-1}	(Quinones and Carpi, 2011)
k_3	Dark-reduction rate constant in soil	1.0×10^{-3} h^{-1}	(Pannu, 2012)
T_f	Reference soil temperature	32°C(Eq.8), 20°C (Eq. 7,9)	(Pannu, 2012;Quinones and Carpi, 2011)
θ_f	Reference soil moisture	25%	(Lin et al., 2010a)
r	Empirical value from regression	0.52	(Lee et al., 2001;Sauve et al., 2000)
s	Empirical value from regression	0.89	(Lee et al., 2001;Sauve et al., 2000)
t	Empirical value from regression	-0.71	(Lee et al., 2001;Sauve et al., 2000)
φ	Ratio of reducible Hg in soil	0.003 (bare), 0.03(others)	(Pannu, 2012)
α_{Hg^0}	Scaling factor of reactivity Hg	0	(Wang et al., 2014b)
β_{Hg^0}	Scaling factor of reactivity Hg	0.1	(Wang et al., 2014b)
Hg_w^{2+}	Hg^{II} concentration on leaf	3 ng m^{-2} leaf	(Laacouri et al., 2013)

805
806

Atmos. Chem. Phys. Discuss., doi:10.5194/acp-2016-314, 2016
Manuscript under review for journal Atmos. Chem. Phys.
Published: 11 May 2016

Atmospheric Chemistry and Physics Discussions

807 Table 2 Examined model variables and the experimental levels of factorial design for air-soil exchange.
808

Terms	Description	Low level	High level
BD	Soil bulk density (g cm^{-3})	0.1	1.5
pH	Soil pH (dimensionless)	4	9
P	Soil total porosity (%)	0.05	0.5
T	Soil temperature (^{o}C)	0	35
SMOIS	Soil moisture (%)	0.05	0.5
R0	Solar irradiance above canopy (w m^{-2})	0	1000
LAI	Leaf area index (dimensionless)	0	7
GEM	Atmospheric Hg0 concentration (ng m^{-3})	1.5	5
Hgs	Hg concentration in soil (ng g^{-1})	10	400
Foc	Soil organic matter content (%)	0.5	30
k1	photo-reduction rates in soil solution ($m^2 W^{-1} s^{-1}$)	3×10^{-9}	9×10^{-9}
k2	photo-reduction rates in soil particles ($m^2 W^{-1} h^{-1}$)	0.7×10^{-3}	3.0×10^{-3}
k3	Non-photo-reduction rates (thermal, h^{-1})	1.0×10^{-3}	2.3×10^{-3}

809

Atmos. Chem. Phys. Discuss., doi:10.5194/acp-2016-314, 2016
Manuscript under review for journal Atmos. Chem. Phys.
Published: 11 May 2016

Atmospheric Chemistry and Physics Discussions

Table 3. Mean annual air-surface fluxes, and annual total Hg emissions from individual landuse. SHg is the Hg content in surface soil (0-10 cm), FF is the Hg^0 flux over foliage, and FS is the Hg^0 flux over soil.

Type	Description	Area(%)	SHg (ng g^{-1})	FF (ng m^{-2} h^{-1})	Leaf(Mg)	FS(ng m^{-2} h^{-1})	Soil(Mg)	Tot(Mg)
C1	Evergreen needleleaf forest	5.7	186±74	-2.8	-13.5	6.9	35.2	21.7
C2	Evergreen broadleaf forest	2.6	184±35	-2.6	-6.5	6.2	16.1	9.5
C3	Deciduous needleleaf forest	0.1	119±9	-0.2	-0.03	0.7	0.1	0.1
C4	Deciduous broadleaf forest	3.3	143±47	-1.2	-3.7	2.7	8.3	4.6
C5	Mixed forest	2.4	211±83	-2.2	-4.5	4.7	10.5	6.0
C6	Closed shrubland	5.2	115±77	-3.2	-14.1	5.6	26.0	11.9
C7	Open shrubland	0.6	155±72	-1.4	-0.7	10.8	6.5	5.7
C8	Woody savanna	0.3	197±96	-4.5	-1.0	12.9	3.2	2.2
C9	Savanna	0.0	157±47	-0.6	-0.003	0.1	0.0	0.0
C10	Grassland	31.8	61±33	-0.8	-20.3	8.0	221.8	201.4
C11	Permanent wetland	1.1	74±24	-0.8	-0.8	9.8	10.0	9.2
C12	Cropland	20.5	80±59	-1.8	-31.6	10.0	179.0	147.5
C13	Cropland mosaic	1.6	82±74	-2.0	-3.0	6.7	10.1	7.2
C14	Urban land	0.2	162±83	-3.6	-0.7	23.3	4.4	3.7
C15	Snow and ice	0.8	31±15			2.0	3.1	3.1
C16	Barren vegetated land	21.6	35±7			1.5	22.2	22.2
C17	Bodies of water	2.2				3.4	9.0	9.0
Sum		100.0			-100.4		565.5	465.1

Atmos. Chem. Phys. Discuss., doi:10.5194/acp-2016-314, 2016
Manuscript under review for journal Atmos. Chem. Phys.
Published: 11 May 2016

Atmospheric Chemistry and Physics Discussions

815 Table 4. Pearson correlations between mean total fluxes and major controlling environmental parameters
816 in each season. "**" means $p < 0.01$ and "*" means $p< 0.05$.
817
818

Term	Winter	Spring	Summer	Autumn
LAI	-0.14*	-0.24**	-0.39**	-0.30**
Soil temperature	0.27**	0.35**	0.54**	0.38**
Solar radiation	0.27**	0.32**	0.59**	0.36**
Soil Hg concentration	0.47**	0.13*	0.02	0.39**
Soil bulk density	0.41**	0.16*	0.04	0.32**

Atmos. Chem. Phys. Discuss., doi:10.5194/acp-2016-314, 2016
Manuscript under review for journal Atmos. Chem. Phys.
Published: 11 May 2016

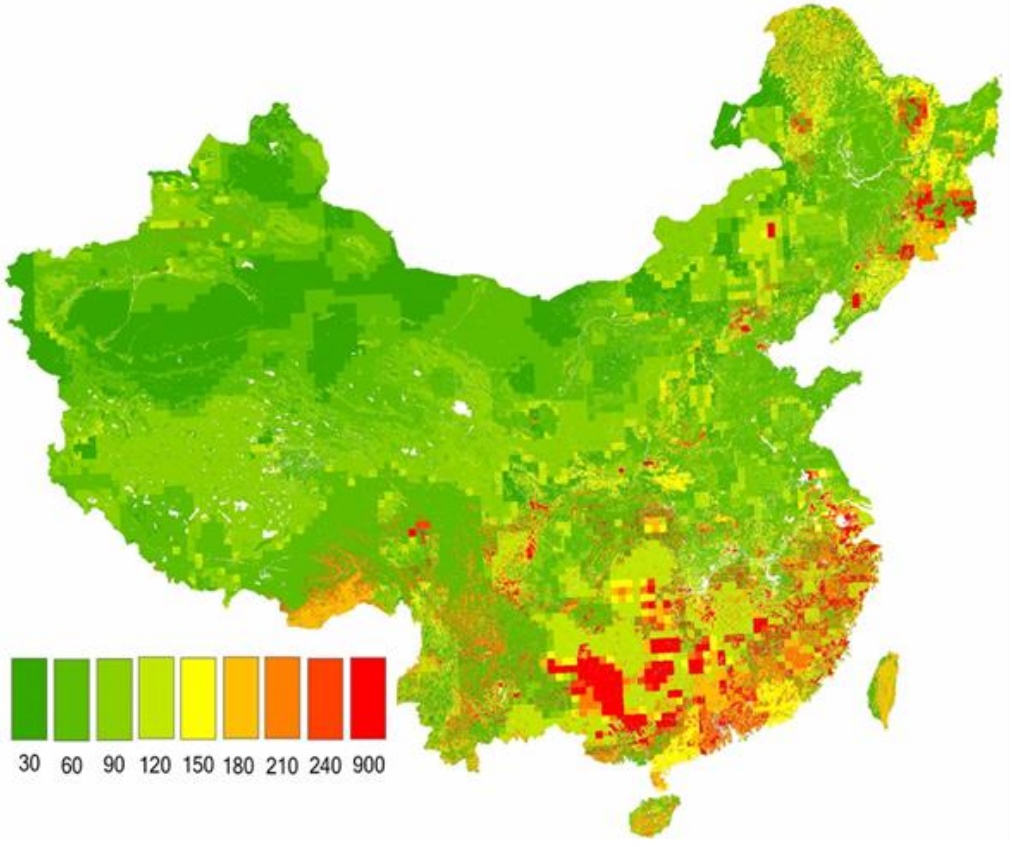

819
820 Figure 1. Updated Hg concentrations (ng g^{-1}) in surface soil of China. Sampling areas in NMPRGS covers
821 most agriculturally and industrially developed regions of eastern and central China, and is presented in
822 more details in Li et al. (2014).
823

Atmos. Chem. Phys. Discuss., doi:10.5194/acp-2016-314, 2016
Manuscript under review for journal Atmos. Chem. Phys.
Published: 11 May 2016

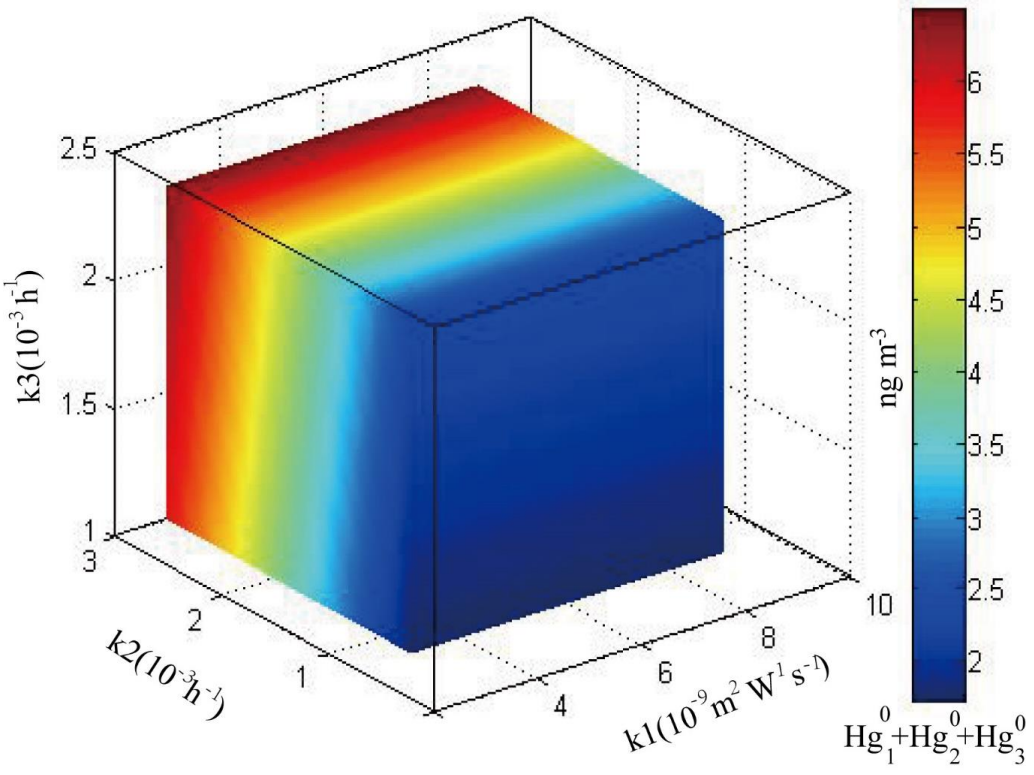

Figure 2. Variation of Hg^0 concentrations in the forest soil pore gas using the typical ranges of kinetic constants for Hg^{II} reduction in soil (see text for details): k_1 = 3.0-9.0×10^{-9} m^2 W^{-1} s^{-1}, k_2 = 0.7-3.0×10^{-3} m^2 W^{-1} h^{-1}, k_3 = 1.0-2.3×10^{-3} h^{-1}, soil Hg content=150 ng g^{-1}, pH=5, soil organic content = 20%, soil bulk density = 0.7 g m^{-3}, solar irradiance = 1000 W m^{-2}, soil temperature = 25 °C, LAI = 5 m^2 m^{-2}, soil moisture content = 20%, and soil soil porosity = 40%.

Atmos. Chem. Phys. Discuss., doi:10.5194/acp-2016-314, 2016
Manuscript under review for journal Atmos. Chem. Phys.
Published: 11 May 2016

Atmospheric Chemistry and Physics Discussions

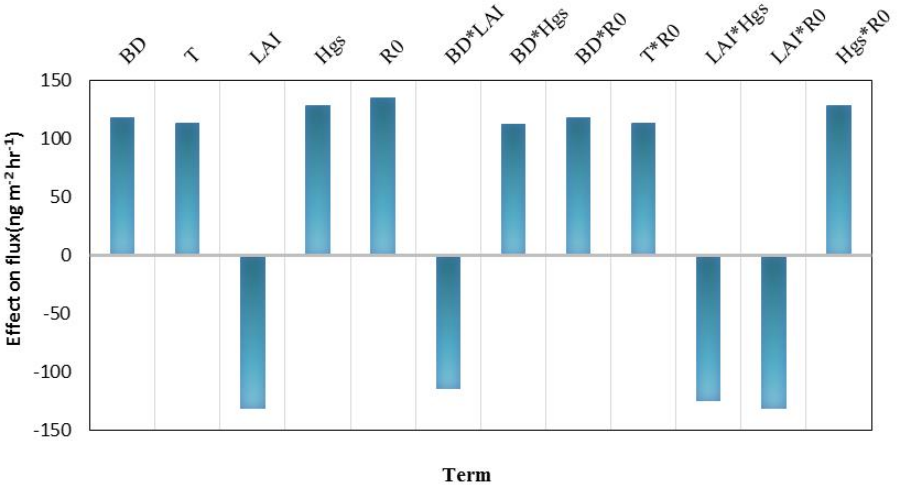

Figure 3. Sensitivity analysis on model parameters for air-soil exchange using a 2-level factorial design after pre-screening the model variables shown in Table 2 for the identified significant factors. The effects shown in the figure is based on a significance level of 95% (i.e., $p<0.05$).

Atmos. Chem. Phys. Discuss., doi:10.5194/acp-2016-314, 2016
Manuscript under review for journal Atmos. Chem. Phys.
Published: 11 May 2016

Atmospheric Chemistry and Physics Discussions

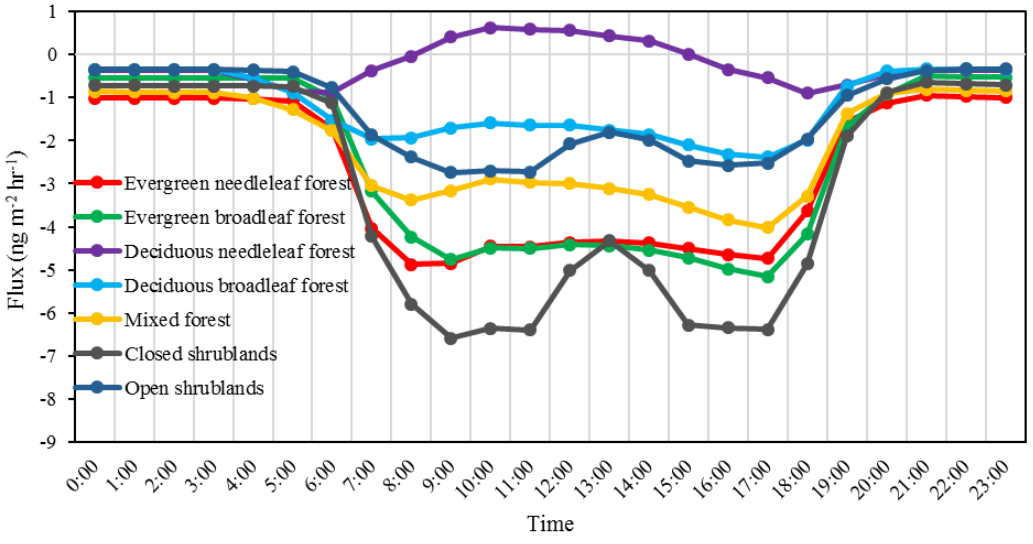

837

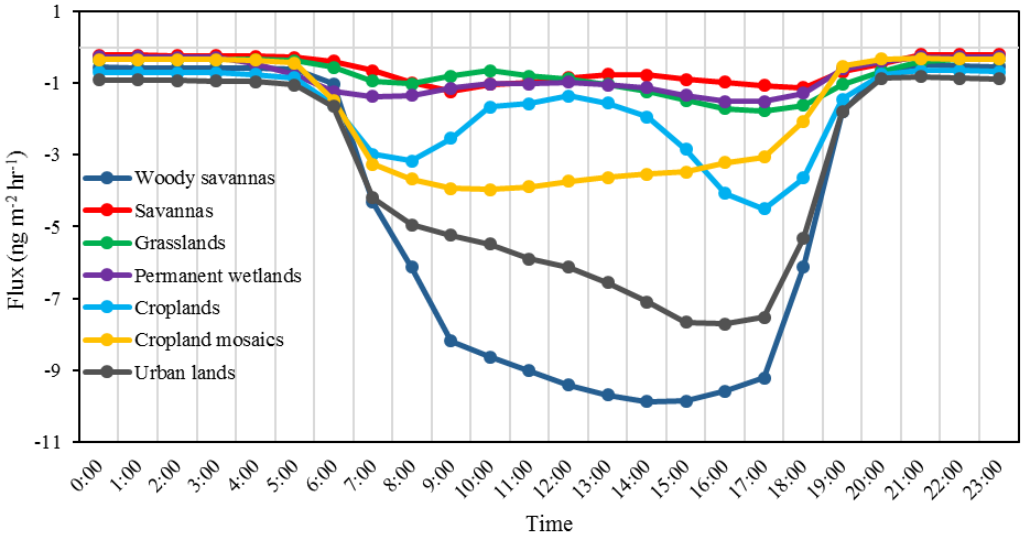

838

839 Figure 4. Diurnal variation of mean simulated exchange fluxes of Hg^0 over canopy in the model domain
840 (UTC+8).

841

842

Atmos. Chem. Phys. Discuss., doi:10.5194/acp-2016-314, 2016
Manuscript under review for journal Atmos. Chem. Phys.
Published: 11 May 2016

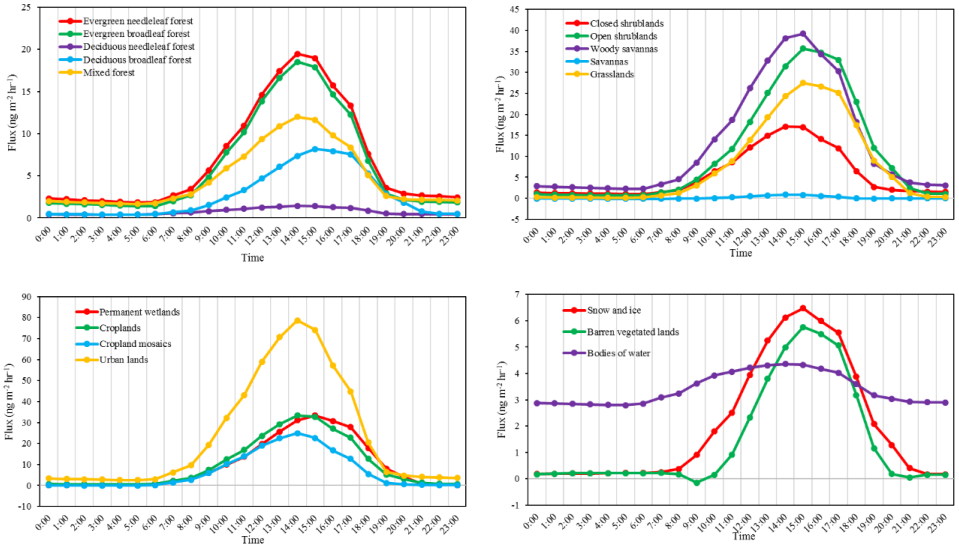

Figure 5. Diurnal variation of mean simulated exchange fluxes of Hg^0 over soil and water surfaces in the model domain (UTC+8).

Atmos. Chem. Phys. Discuss., doi:10.5194/acp-2016-314, 2016
Manuscript under review for journal Atmos. Chem. Phys.
Published: 11 May 2016

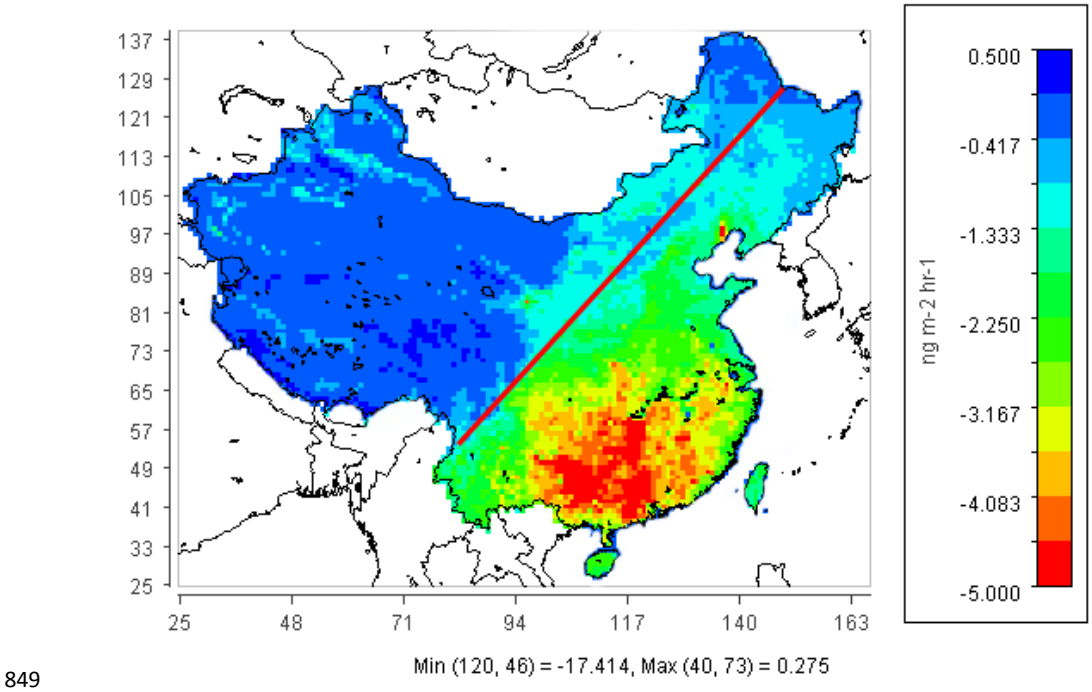

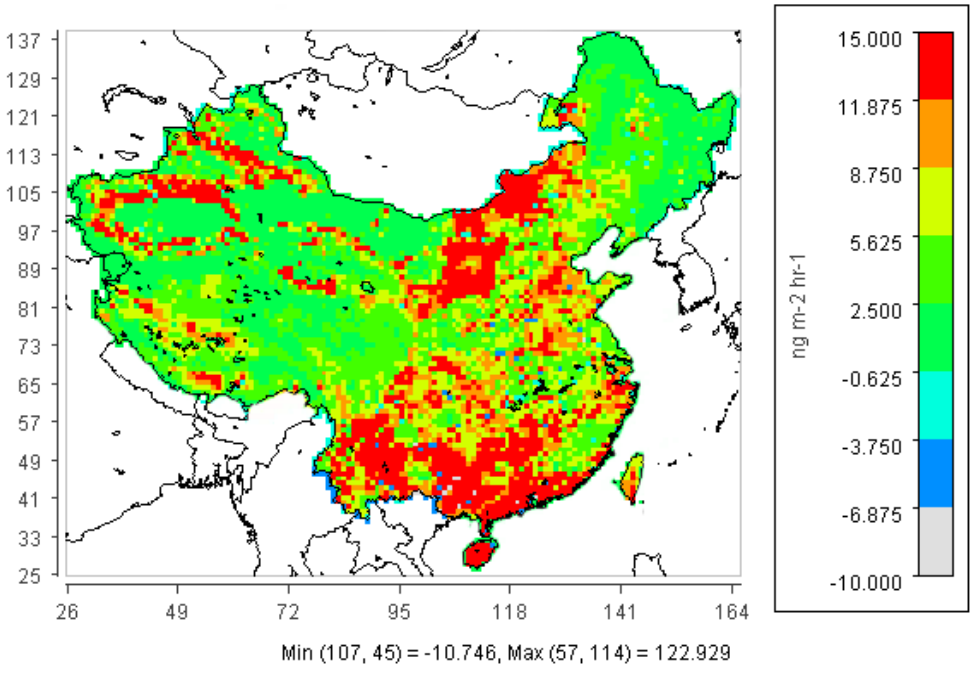

Figure 6. Simulated results of (1) mean annual air-foliage flux, and (2) mean annual air-soil flux in the study domain.

Atmos. Chem. Phys. Discuss., doi:10.5194/acp-2016-314, 2016
Manuscript under review for journal Atmos. Chem. Phys.
Published: 11 May 2016

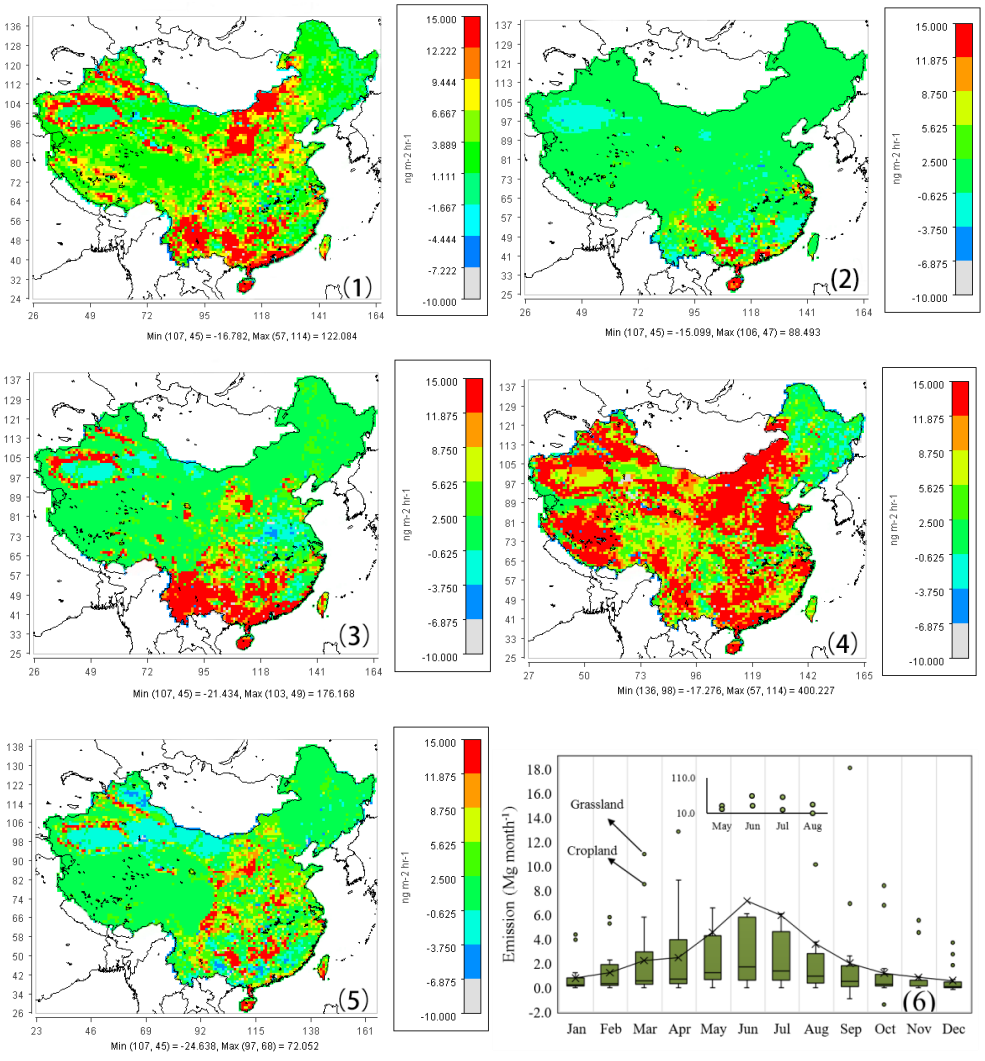

Figure 7. Model estimates of (1) annual mean Hg^0 fluxes in the model domain; (2) seasonal mean Hg^0 fluxes in winter, (3) seasonal mean Hg^0 fluxes in spring, (4) seasonal mean Hg^0 fluxes in summer, (4) seasonal mean Hg^0 fluxes in autumn, and (6) monthly Hg^0 fluxes in the grid cells (box and whisker chart showing maximum, 75th percentile, mean, median, 25th percentile, and minimum).

Atmos. Chem. Phys. Discuss., doi:10.5194/acp-2016-314, 2016
Manuscript under review for journal Atmos. Chem. Phys.
Published: 11 May 2016

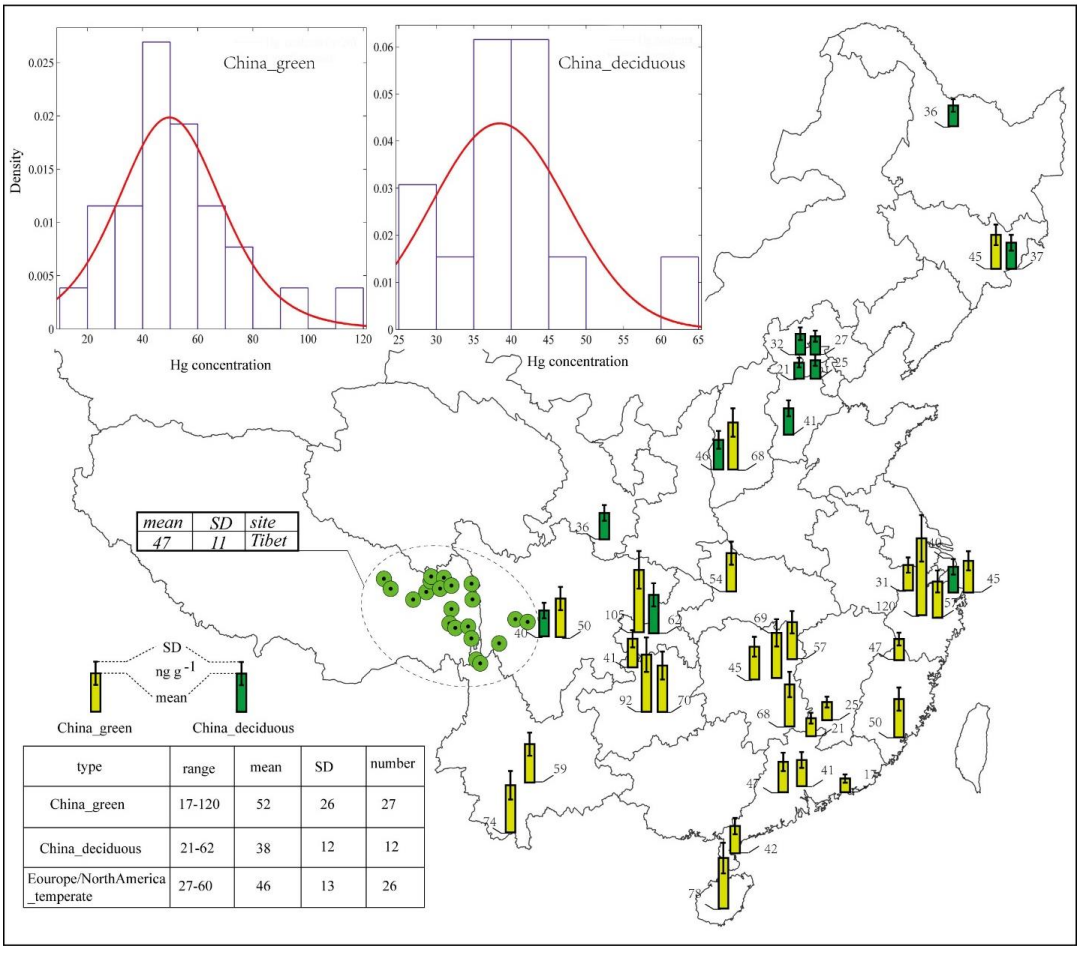

type	range	mean	SD	number
China_green	17-120	52	26	27
China_deciduous	21-62	38	12	12
Eourope/NorthAmerica _temperate	27-60	46	13	26

Figure 8. Database of Hg concentration in litterfall samples, China (Ma et al., 2015;Niu et al., 2011;Zhou et al., 2013;Fu et al., 2015;Wang et al., 2014a;Tang et al., 2015;Juillerat et al., 2012;Blackwell et al., 2014;Risch et al., 2012;Selvendiran et al., 2008). An unpublished dataset including 8 sites in China is described in details in the SI. The Hg concentrations in evergreen and deciduous forests have a t Location-Scale distribution (μ=50.1, σ=19.3, F=6.6; and μ=36.3, σ=3.6, F=1.4, respectively).

Atmos. Chem. Phys. Discuss., doi:10.5194/acp-2016-314, 2016
Manuscript under review for journal Atmos. Chem. Phys.
Published: 11 May 2016

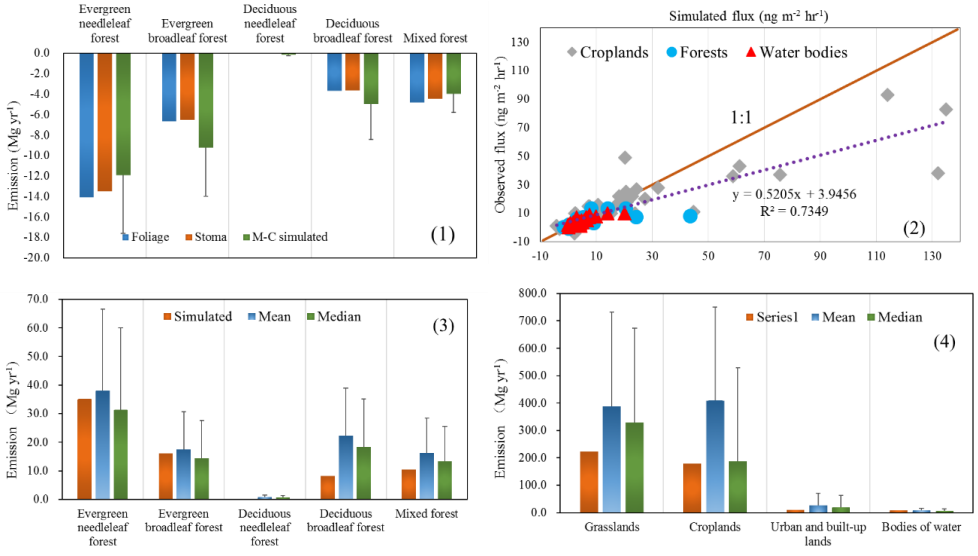

Figure 9. Model verification: (1) model estimates of Hg^0 uptake by foliage (which include the uptake by stoma less the re-emission and from cuticle) and by stoma, compared to the estimate (mean and 95% confidence interval) of Hg^0 uptake using Monte Carlo (M-C) simulation of the observational data; (2) scatter plot of the observed fluxes vs. simulated fluxes for different landuses (the flux observations are described in detailed in Table S2), (3) comparison between simulated exchange and measured exchange over soil under canopy, and (4) comparison between simulated exchange and measured exchange over grasslands, cropland and water surface. The mean and median of Figure 9.3 and 9.4 are based on the filed data from peer-review literatures (n=19 for forests; n=12 for grasslands; n=42 for croplands; n=51 for water bodies). Note that the exchange over deciduous forests in Figure 9.1 is small because of the small forest area.